11. Principles of helioseismology: Local helioseismology

Randomly excited solar oscillations

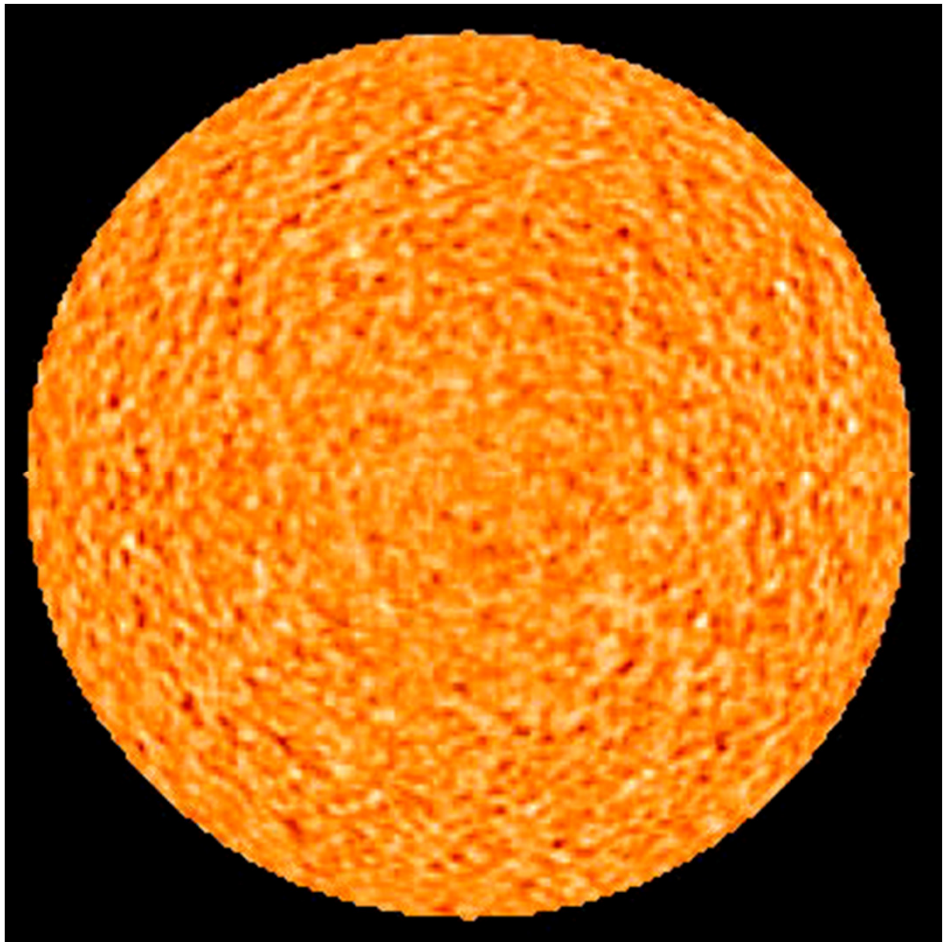

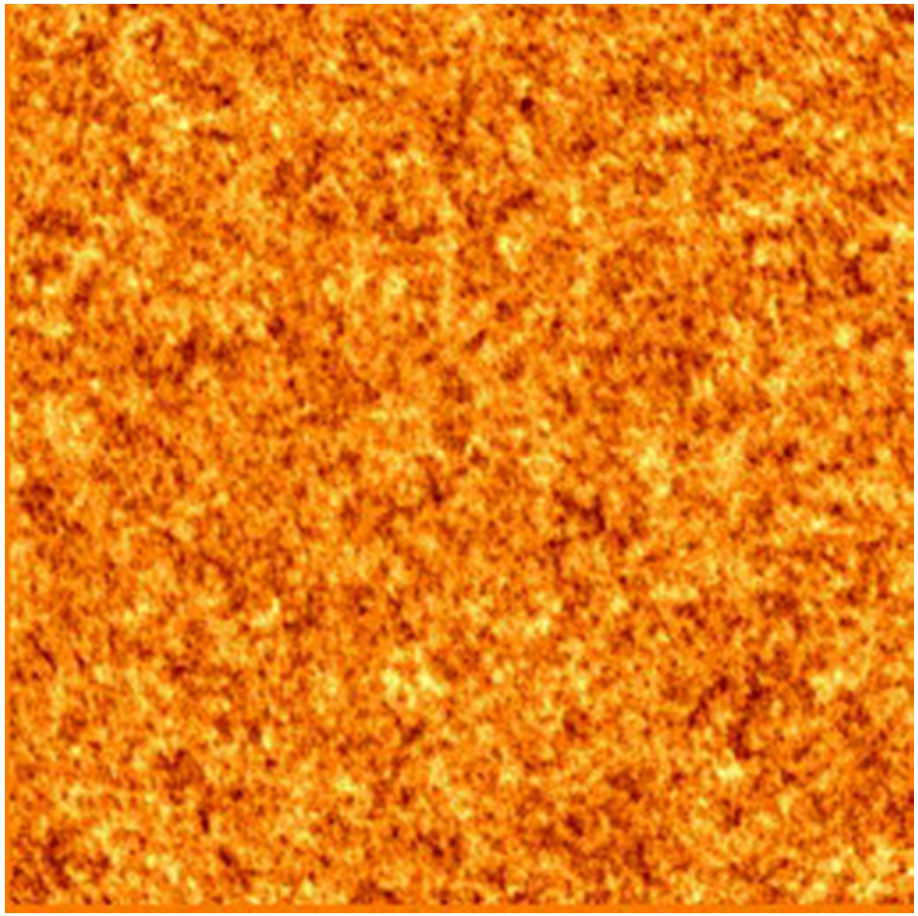

The idea of helioseismology

- Measure travel times τ or resonant frequencies ω of acoustic waves and infer the internal properties, e.g. $c_s(r)$ - sound speed

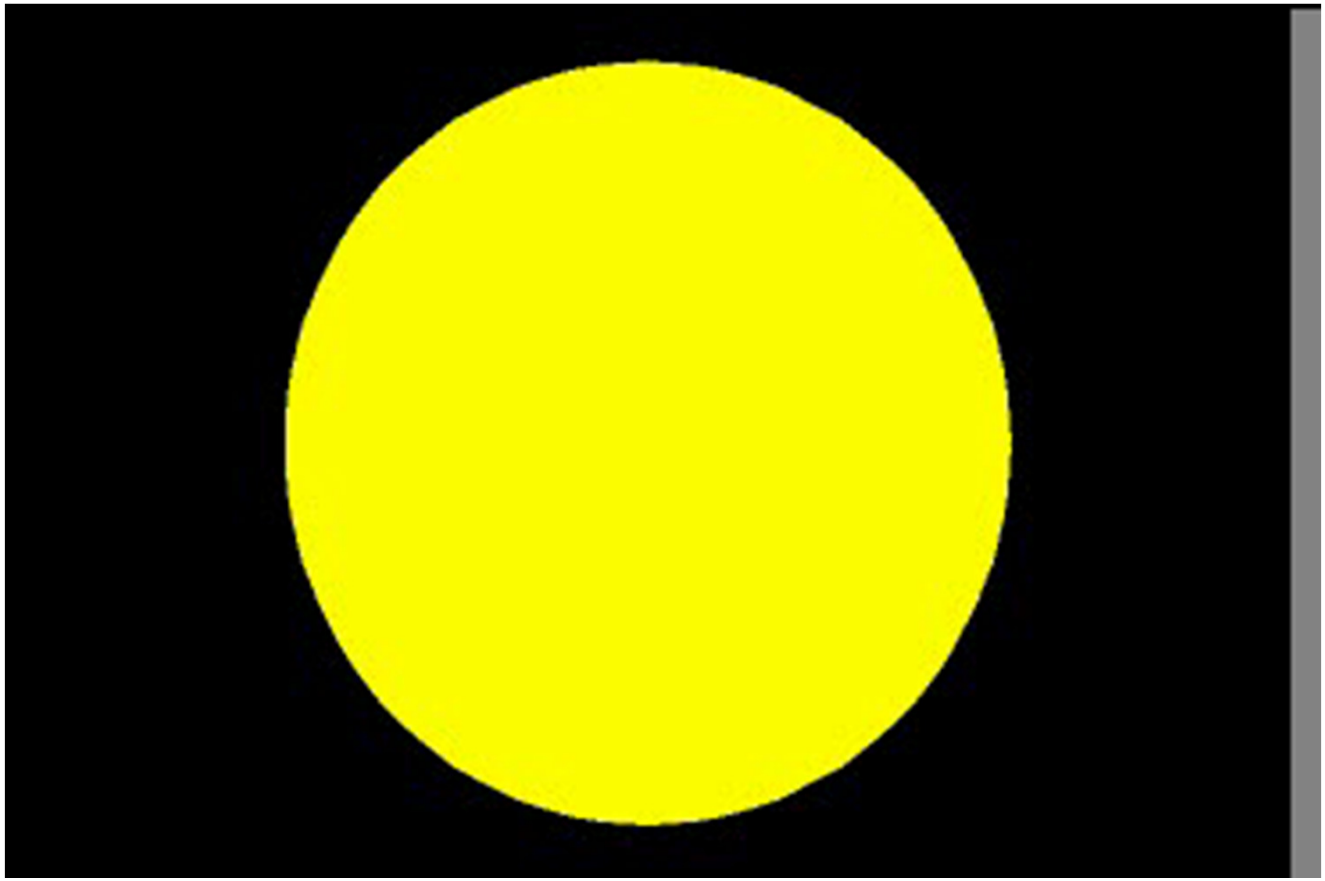

Two principal approaches

- Global Helioseismology – measure global oscillation modes from the oscillation power spectra obtained by applying the spherical harmonic transform to the full-disk oscillation data
- Local Helioseismology - measure variations of oscillation frequencies in local areas by applying the Fourier transform to the oscillations in these area, or by measuring the travel times of phase shifts in local areas.

Methods of local-area helioseismology:

Method	Observable	Inferences
Ring-diagram analysis (Gough, Hill, November, Toomre, 1981)	Local variations of oscillation frequencies	Large-scale sound speed perturbations and horizontal flows
Time-distance helioseismology (Duvall et al. 1993)	Phase and group travel times of acoustic and surface gravity waves	3D sound speed, density and flows
Acoustic Imaging (Chou, LaBonte, et al. 1990)	Phase and amplitude variations	3D sound speed and flows
Acoustic Holography (Lindsey & Braun, 1990)	Phase and amplitude variations	Phase variations and amplitude maps

Input Data

Dopplergrams-

observational requirements:

- long duration (>4 hours)
- high-resolution (0.5 arcsec per pixel)
- high-cadence (45-sec cadence)
- stability

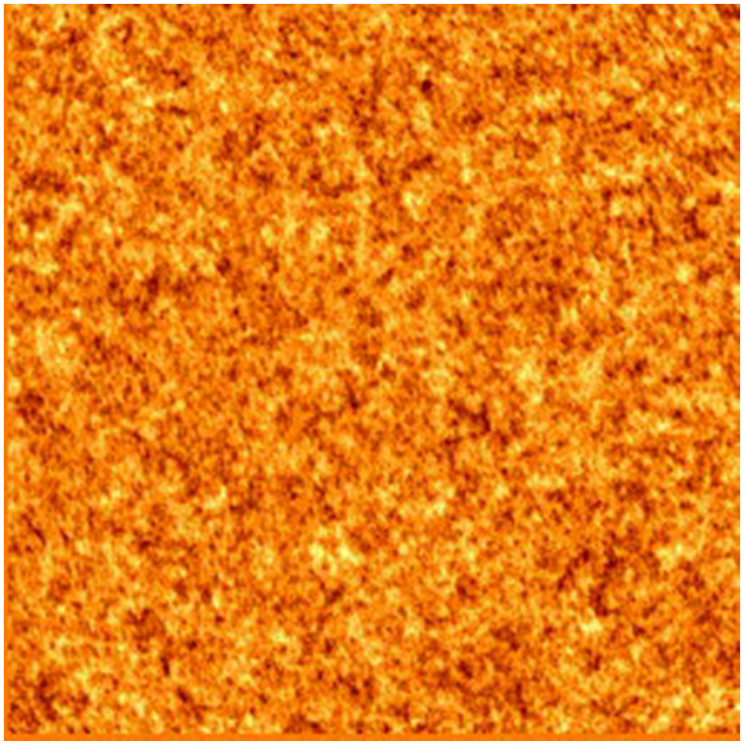

SDO high-resolution Dopplergrams

3D Power Spectrum

Velocity of oscillations $v(x, y, t)$ can be represented in terms of its Fourier components:

$$a(k_x, k_y, \omega) = \iiint v(x, y, t) e^{i(k_x x + k_y y + \omega t)} dx dy dt,$$

where k_x and k_y are components of the wave vector, ω is the frequency.

The power spectrum is:

$$P(k_x, k_y, \omega) = a^* a,$$

where a^* is complex conjugate.

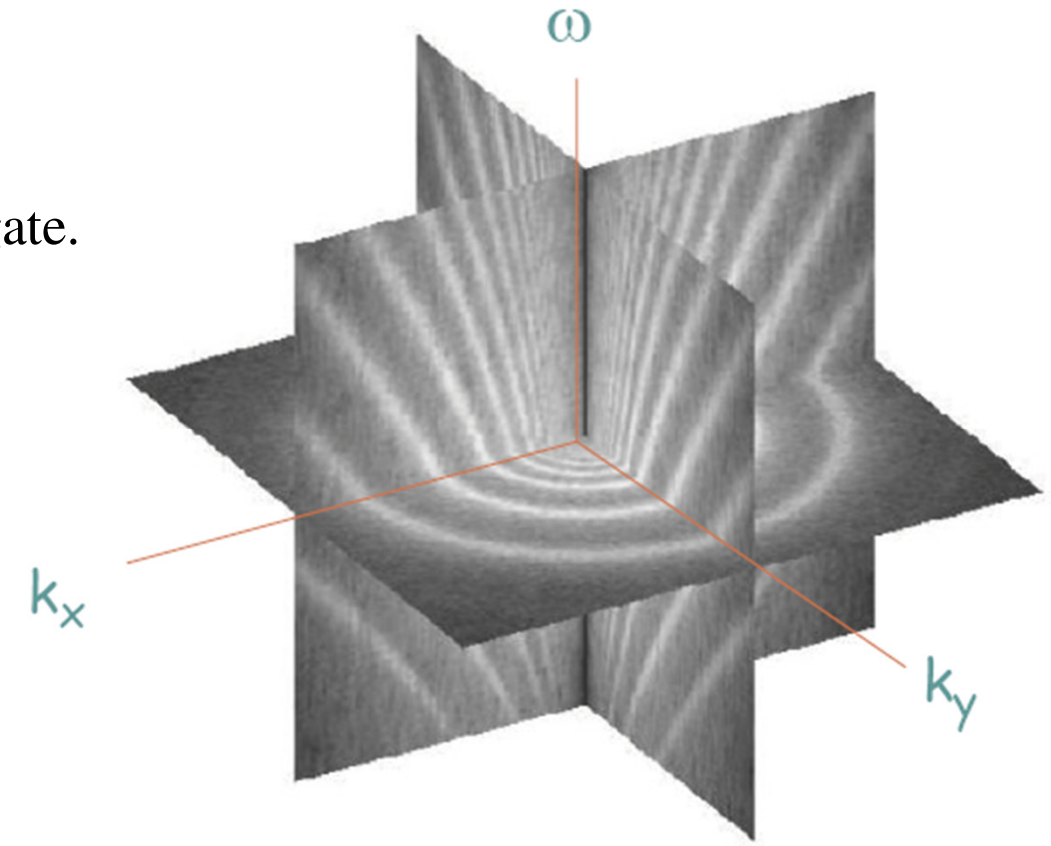

Compare with the global oscillation power spectrum

Spectrum of global oscillations of the sphere

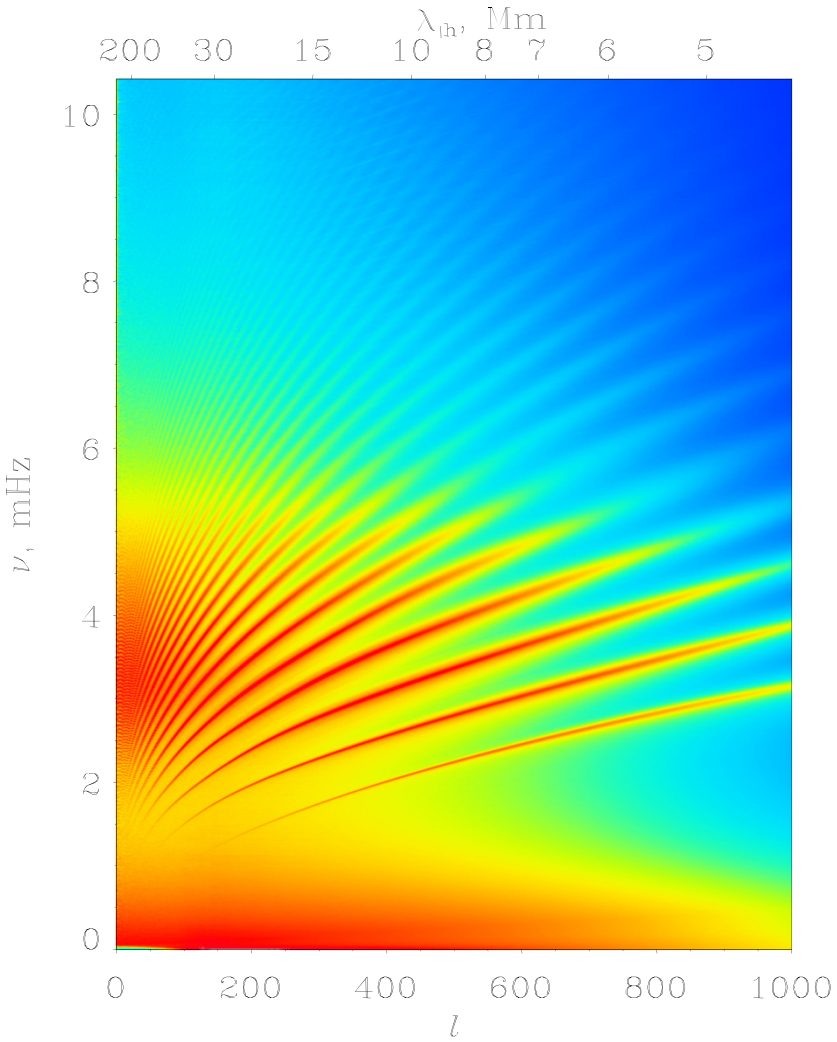

Spectrum of oscillations in a local area

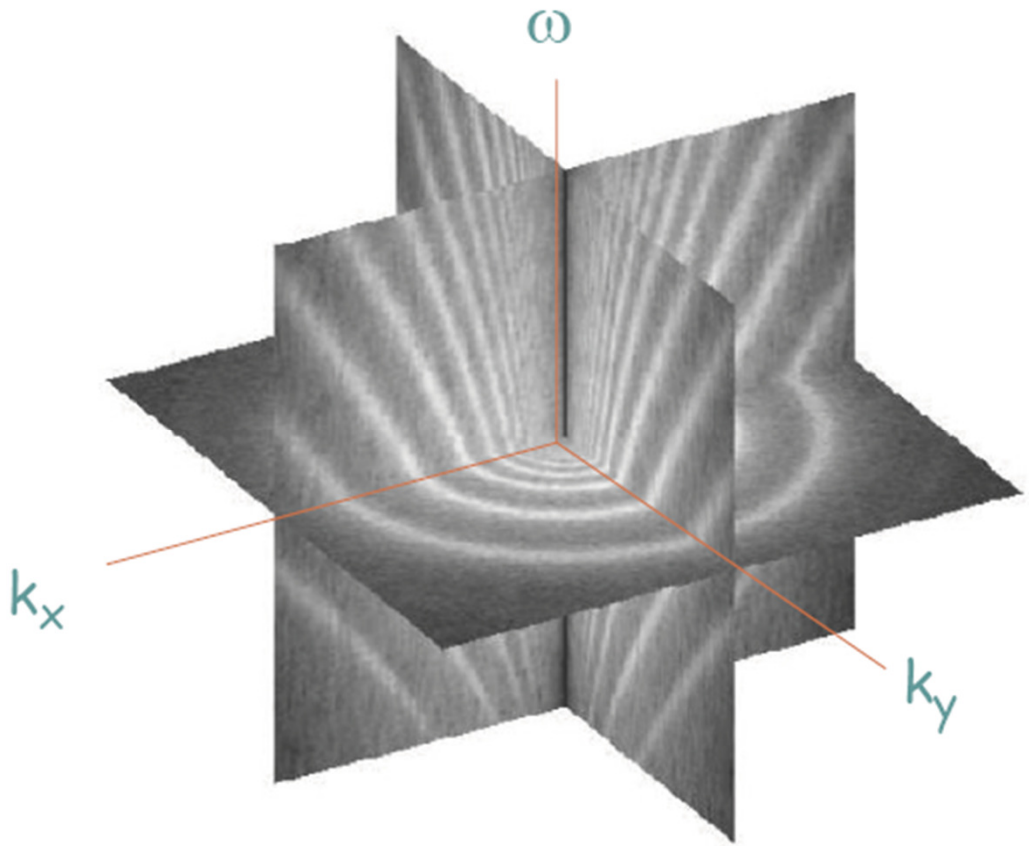

Cuts of the local power spectra at constant frequencies produce rings

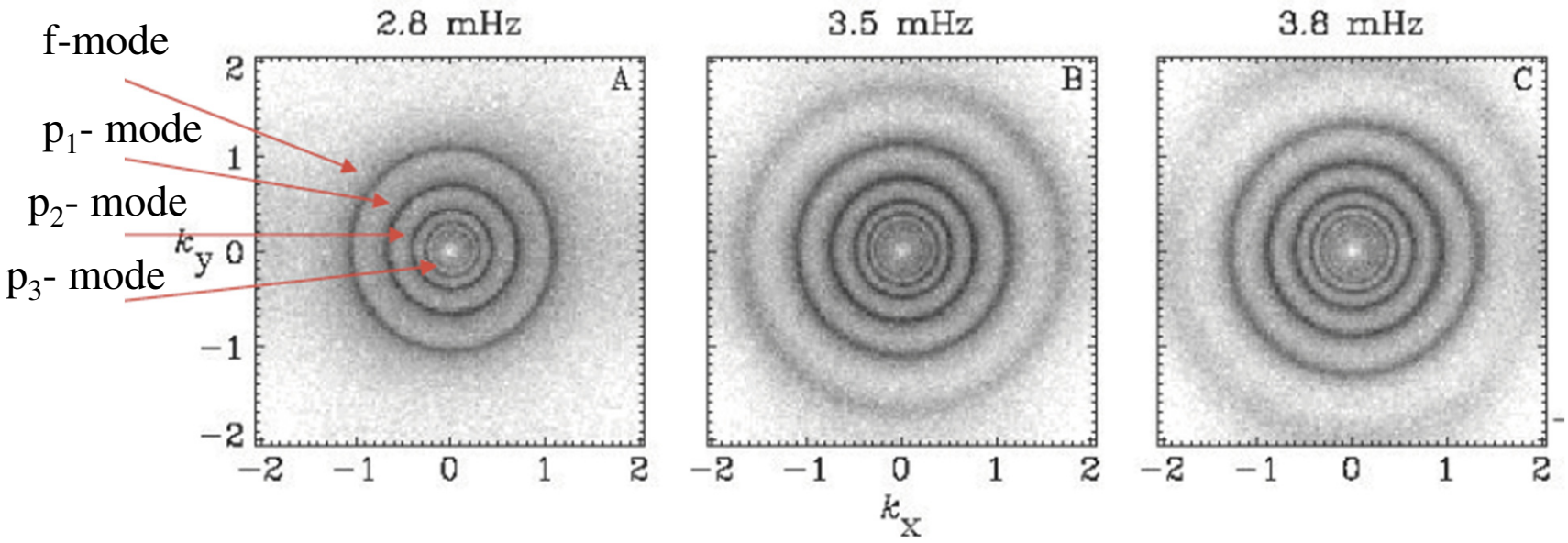

Flows cause displacement of rings (Doppler shift of solar waves)

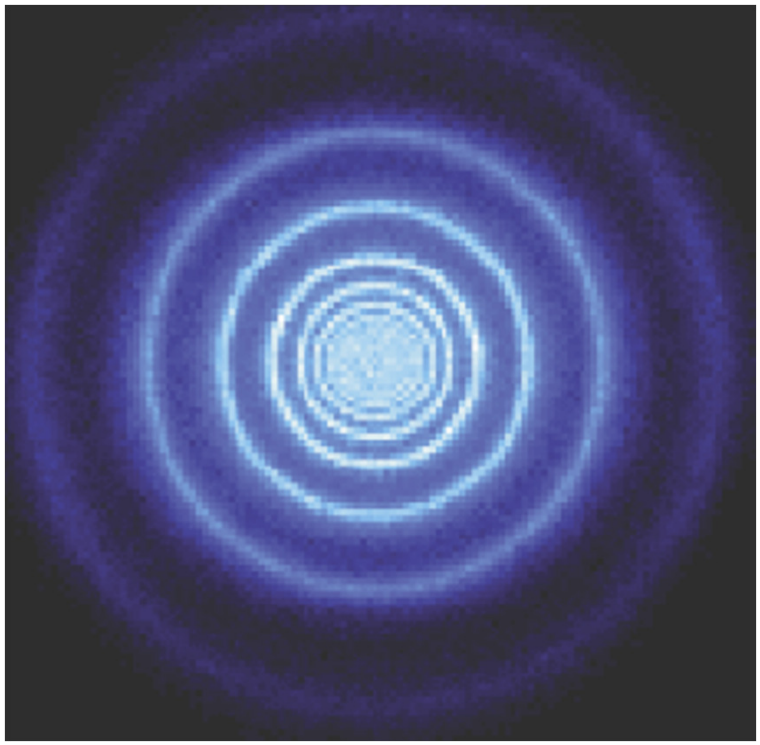

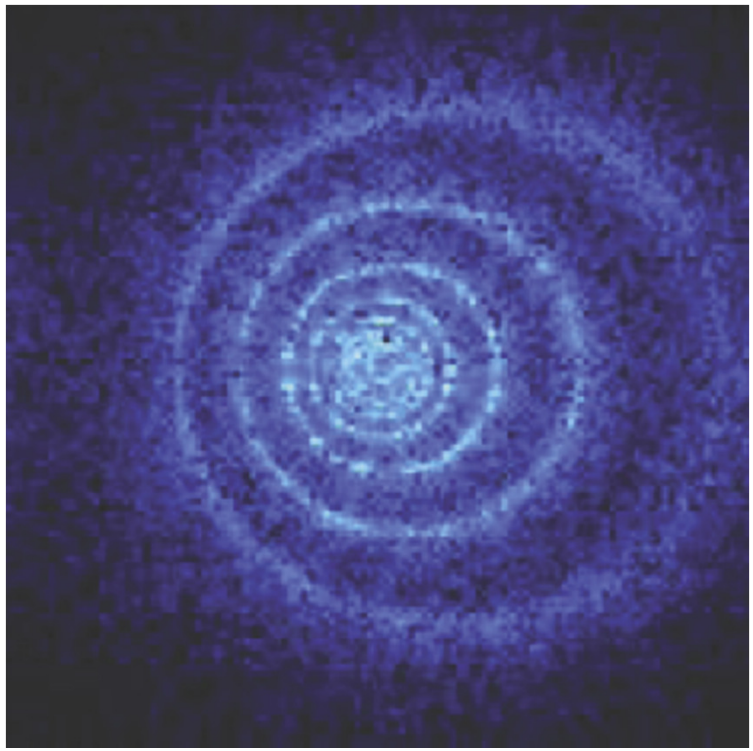

$$(\omega - k_x U)^2 = \omega_c^2 + c^2 k^2$$

Frequency shift caused by flow with velocity U along x-axis. By measuring the shift for various modes one can determine the depth dependence of U.

Ring-Diagram Analysis

The ring-diagram method is based on inversion of the local dispersion relation (3D power spectrum) for acoustic waves.

Perturbation to the local variation in frequency of the component of the wave pattern whose local horizontal wave number is k is given by

$$\frac{\Delta\omega}{\omega} = \frac{\vec{k}}{\omega}\int B\vec{U}dz + \int F\frac{\delta c^2}{c^2}dz + \int G\frac{\delta\gamma}{\gamma}dz$$

$\vec{U}$ is the horizontal component of flow velocity, $\delta c^2/c^2$ and $\delta\gamma/\gamma$ are perturbations to the local sound speed and adiabatic exponent; B(z), F(z), and G(z) are the sensitivity functions that are similar to the global helioseismology Using this equation one can infer the horizontal flow velocity and sound-speed perturbations averaged over some areas (15^ox15^o) as a function of depth z.

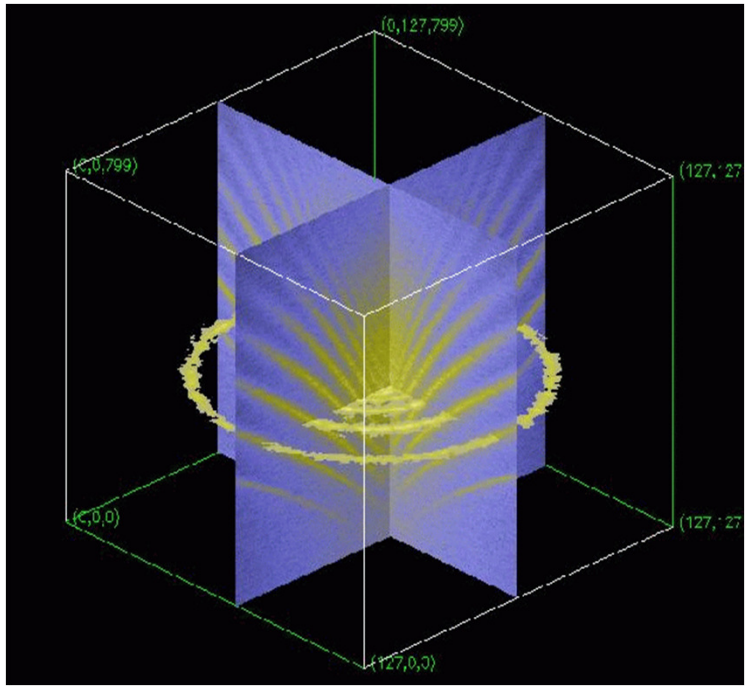

Local 3D power spectrum of acoustic waves as a function of horizontal wave numbers k_x, k_y (horizontal axes) and frequency ω (vertical axis).

Time-distance helioseismology

Measures travel times of acoustic or surface gravity waves propagating between different surface points through the interior. The travel times τ depend on conditions, flow velocity U and sound speed variations c along the ray path Γ.

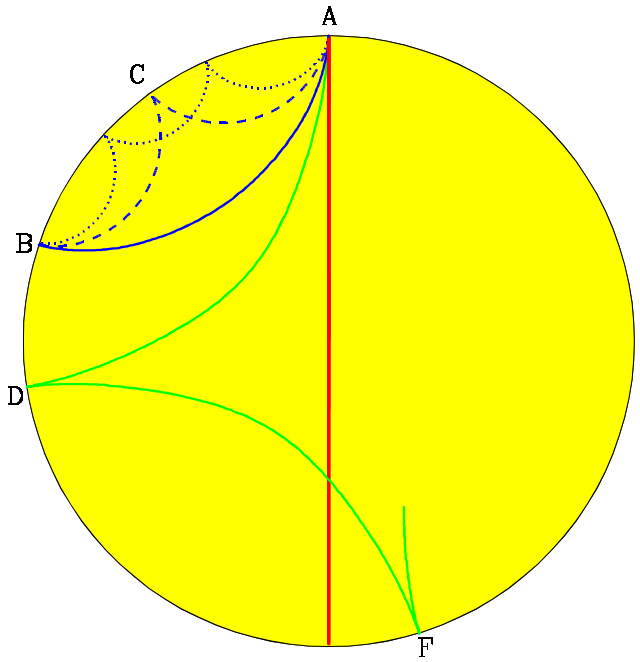

In practice, travel-time variations are measured:

$$\delta\tau = -\int_{\Gamma} \frac{k}{\omega}\frac{\delta c}{c} ds - \int_{\Gamma} \frac{\left(\vec{n}\cdot\vec{U}\right)}{c^2} ds$$

ω/k is the wave phase speed

$\vec{n}$ is a unit vector along the ray path.

Time-distance diagnostics

- Using the time-distance diagram one can measure the travel time of acoustic waves for various distances, and then infer the sound speed along the wave paths.
- Can we measure the travel times by using the stochastic wave field continuously generated by the turbulent convection?

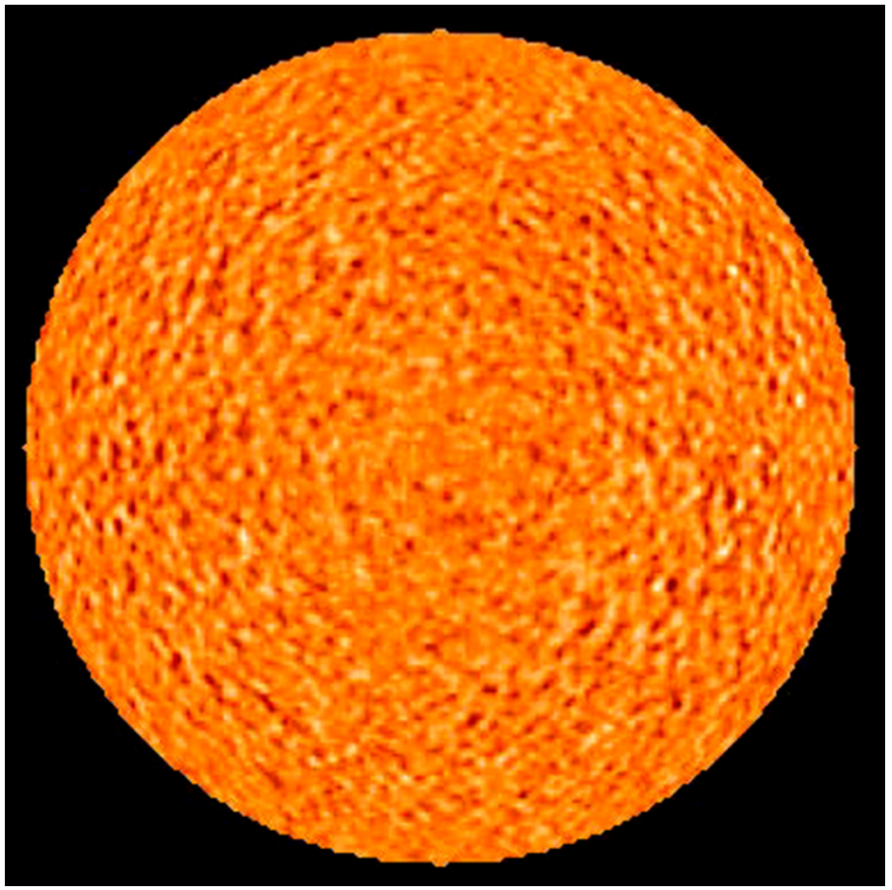

Time-distance helioseismology

A remarkable discovery was made by Tom Duvall in 1993 that the travel times of the solar waves can be measured by using a cross-covariance function of the stochastic wave field:

$$\psi(\tau,\Delta) = \int_0^T f(t,r) f^*(t+\tau, r+\Delta) dt$$

or $C(\tau,\Delta)$

Integration time

Time

Distance

Oscillation signal (Doppler velocity, intensity etc) at two points on the Sun's surface

Time-distance measurements

Travel times are determined from the cross-covariance function:

$$\psi(\tau,\Delta)=\int_0^T f(t,r)\,f^*(t+\tau,r+\Delta)\,dt$$

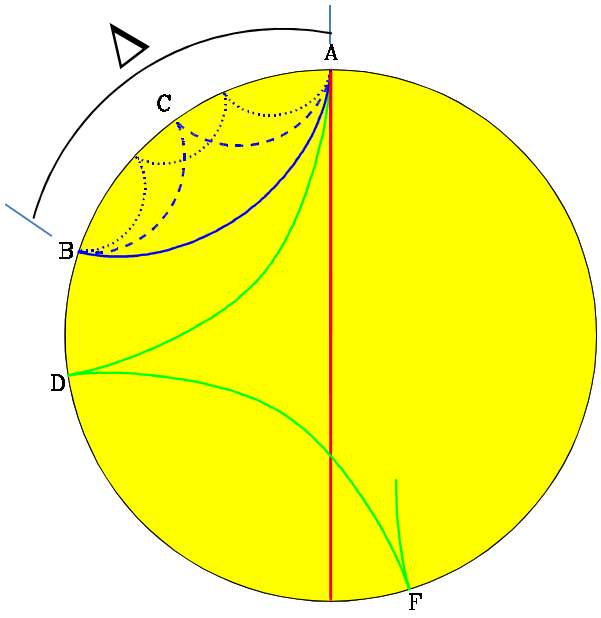

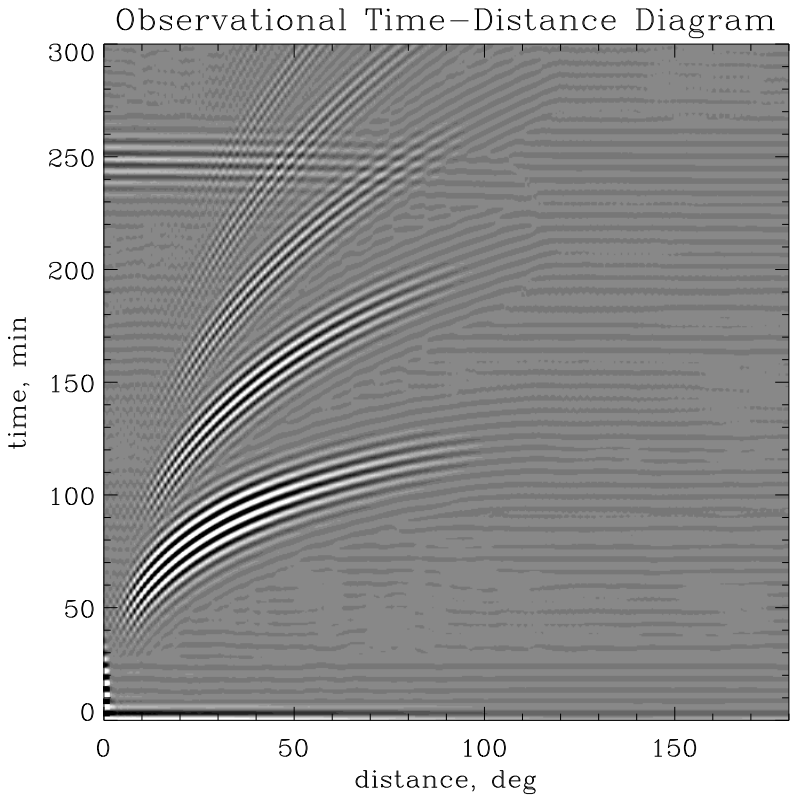

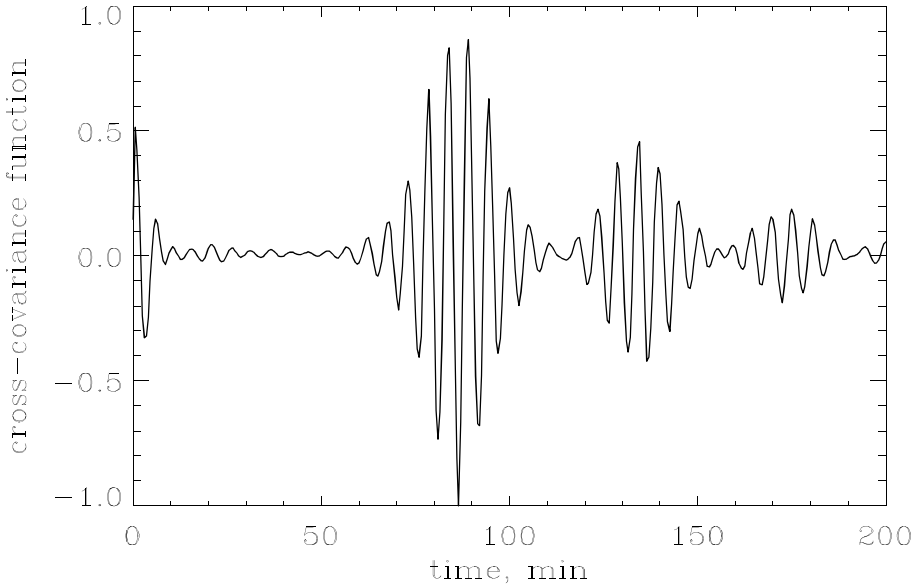

Cross-covariance function for a particular distance (30 degrees in this case) represents a series of wave packets.

Simple interpretation of time-distance measurements

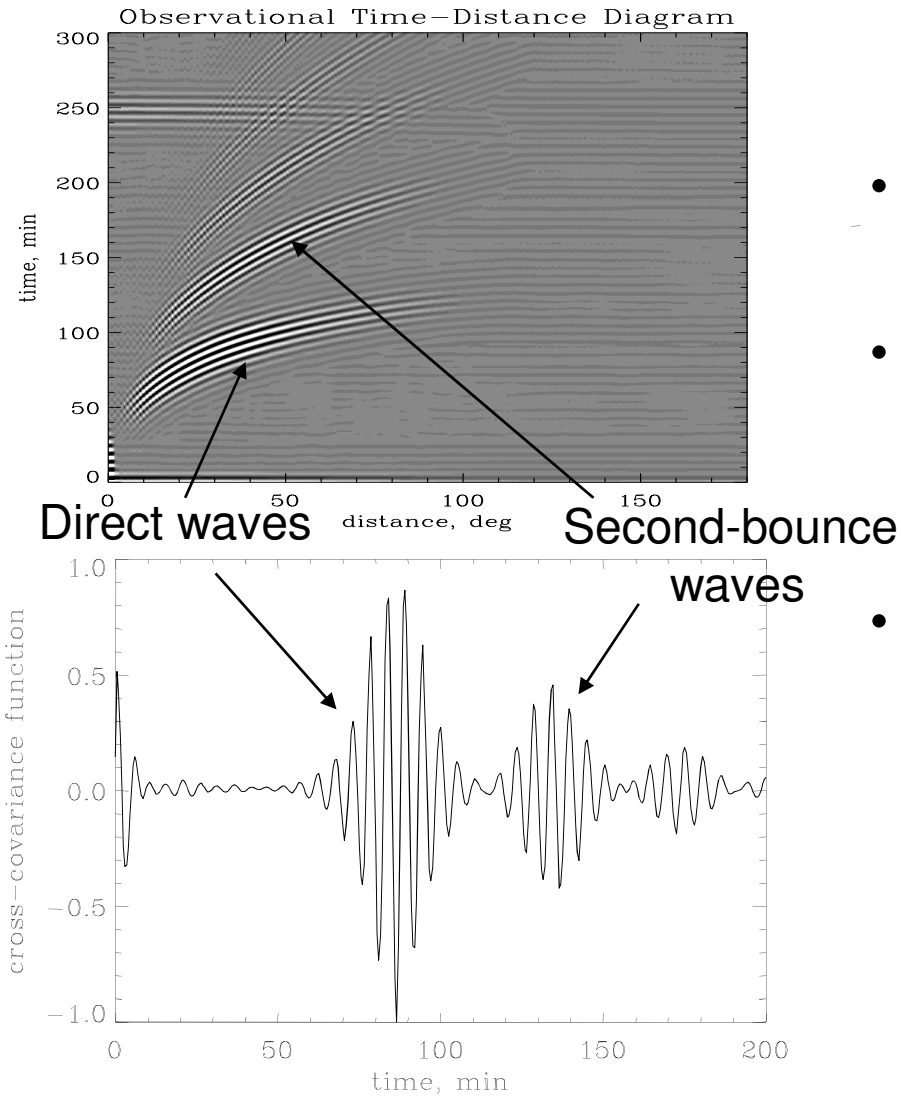

- The cross-covariance function collects coherent signals for solar waves excited at a given point and traveling to another point
- The cross-covariance signal corresponds to a strong point source (similar to the flare signal) – Claerbout's conjecture
- The cross-covariance signal corresponds to a wave packet of waves in a finite frequency range. The solar oscillations have periods around 5 min. Thus, we see the 5-min periodicity in the wave packet.
- The cross-covariance function can be used for measuring group and phase travel times.

We measure the group and phase travel times from these diagrams.

Time-distance inferences of the sound speed and flow velocity

Measures travel times of acoustic or surface gravity waves propagating between different surface points through the interior. The travel times depend on conditions, flow velocity and sound speed along the ray path:

$$\delta\tau = -\int_{\Gamma} \frac{k}{\omega}\frac{\delta c}{c} ds - \int_{\Gamma} \frac{\left(\vec{n}\cdot\vec{U}\right)}{c^2} ds$$

The sound speed and flow velocity signals are separated by measuring the travel times for waves propagating in the opposite directions along the same ray paths and calculating the mean travel times and the differences:

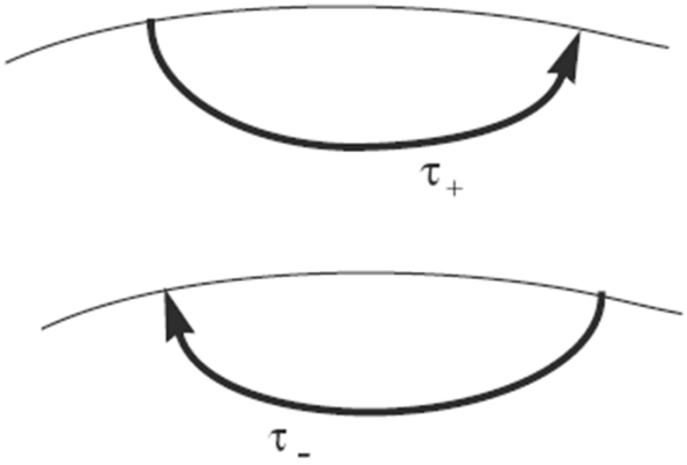

$$\delta\tau_{\text{mean}} = \frac{1}{2}(\tau_+ + \tau_-) = -\int_{\Gamma} \frac{k}{\omega}\frac{\delta c}{c} ds$$

$$\delta\tau_{\text{diff}} = \tau_+ - \tau_- = -\int_{\Gamma} \frac{\left(\vec{n}\cdot\vec{U}\right)}{c^2} ds$$

Vector velocity measurement scheme

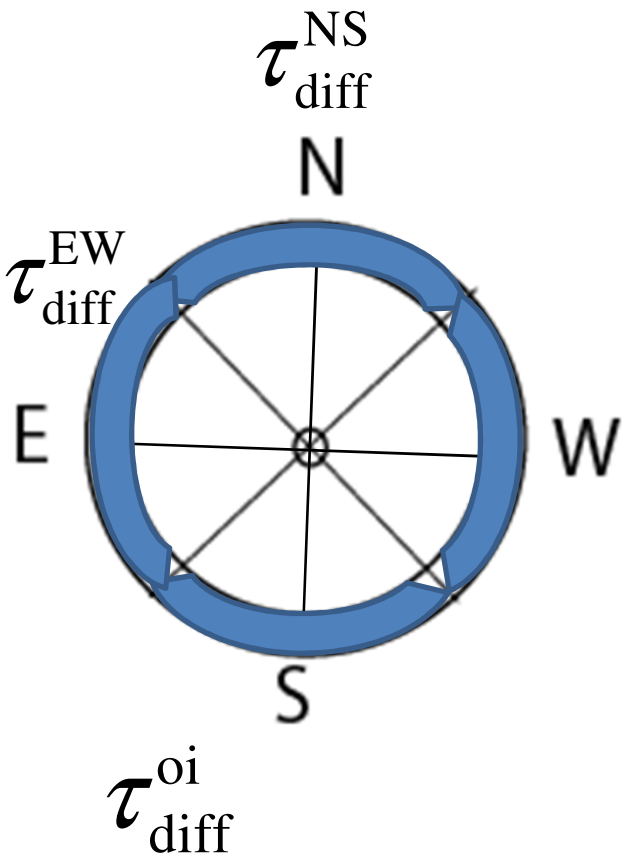

is a travel time difference averaged over the full annulus.

Typically, we measure times for acoustic waves to travel between points on the solar surface and surrounding quadrants symmetrical relative to the North, South, East and West directions. In each quadrant, the travel times are averaged over narrow ranges of travel distance Δ.

Then, the times for northward-directed waves are subtracted from the times for south-directed waves to yield the time, τ^{NS}_{diff}, which predominantly measures north-south motions. Similarly, the time differences, τ^{EW}_{diff}, between westward- and eastward directed waves yields a measure of east-ward motion. The time, τ^{oi}_{diff}, between outward- and inward-directed waves, averaged over the full annuli, is mainly sensitive to vertical motion and the horizontal divergence.

This provides a qualitative picture of the motions, and is useful for a preliminary analysis. However, in numerical inversions, all three components of the flow velocity are properly taken into account. The averaging procedure is essential for reducing noise in the data.

Tomographic Inversion

We assume that the convective structures and flows do not change during the observations and represent them by a discrete model. In the model, the 3D region of wave propagation is divided into rectangular blocks. The perturbations of the sound speed and the three of the flow velocity are approximated by linear functions of coordinates within each block, e.g.

$$\delta c(x,y,z) = \sum c_{ijk}\left[1-\frac{|x-x_i|}{x_{i+1}-x_i}\right]\left[1-\frac{|y-y_j|}{y_{j+1}-y_j}\right]\left[1-\frac{|z-z_k|}{z_{k+1}-z_k}\right]$$

According to the averaging procedure of the cross-covariance function, the travel time measured at a point on the surface is the result of the cumulative effects of the perturbations in each of the traversed rays of the 3D ray systems (see Figure below). Therefore, we average the equations for $\delta\tau$ over the ray systems corresponding to the different radial distance intervals of the data, using approximately the same number of ray paths as in the observational procedure. As a result, we obtain two systems of linear equations that relate the data to the sound speed variation and to the flow velocity, e.g. for the sound speed

$$\delta\tau_{\lambda\mu\nu} = \sum_{ijk} A^{ijk}_{\lambda\mu\nu}\ \delta c_{ijk}$$

where matrix A maps the structure properties into the observed travel time variations, λ and μ define the location of the central point of a ray system on the surface, and ν labels surrounding annuli. The equation is solved by a regularized least-squares technique.

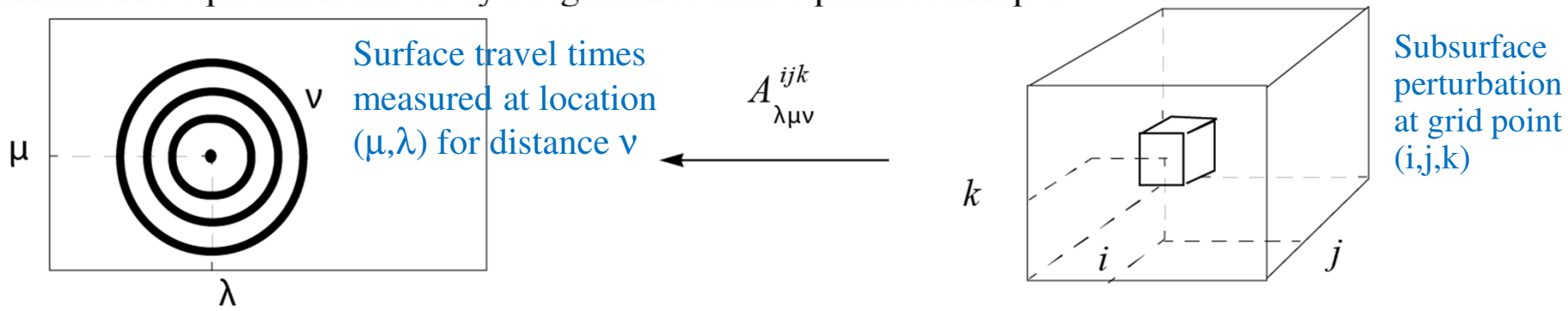

Deep- and surface-focusing observing schemes

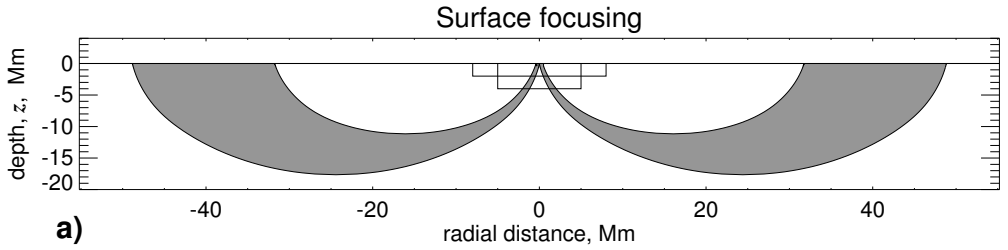

a)

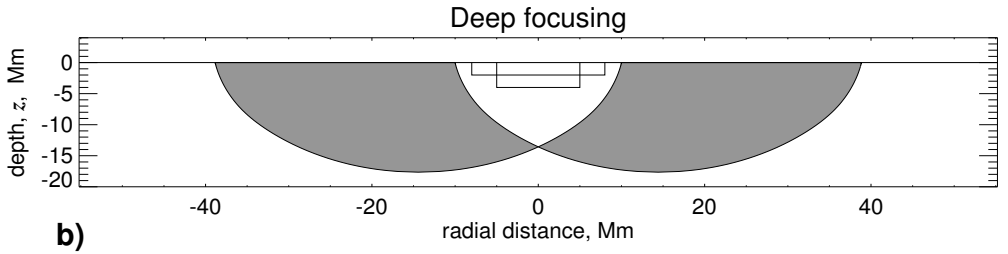

b)

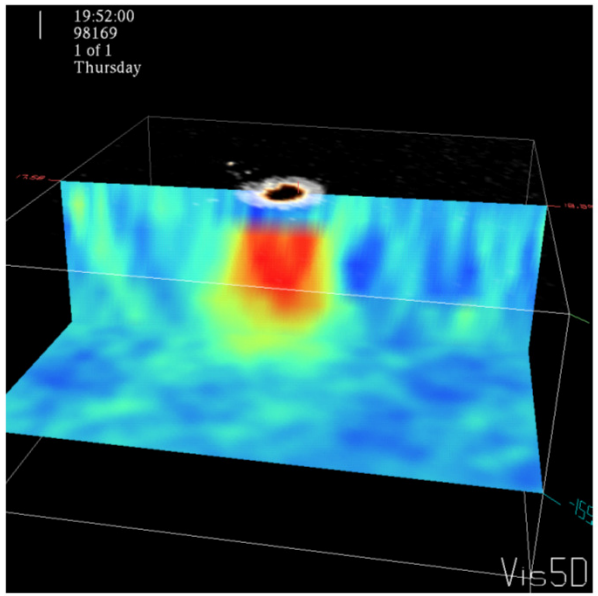

a)

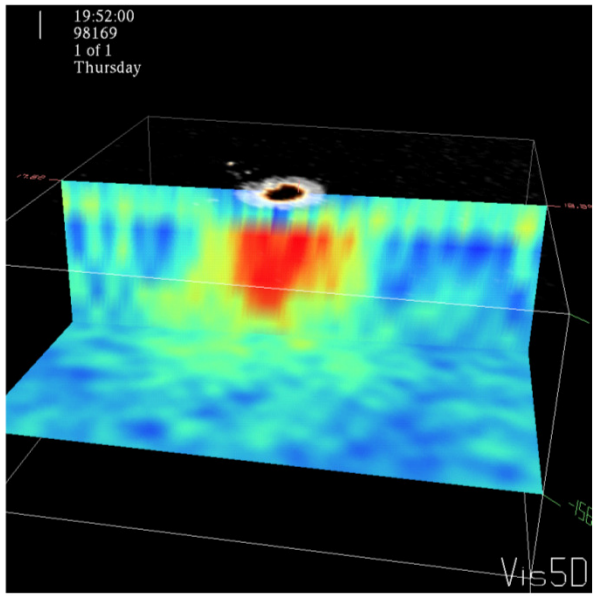

b)

Helioseismic holography

The idea of helioseismic holography is to reconstruct the acoustic wave field at particular locations beneath the surface by using measurements on the surface and a theoretical Green's functions for the wave propagation from point sources.

The ingression and egression estimate of the wave field at some point in the solar interior assuming that the observed wave field resulted entirely from waves diverging from that point (for the egression) or waves converging towards that point (for the ingression). Egression propagates signals back in time.

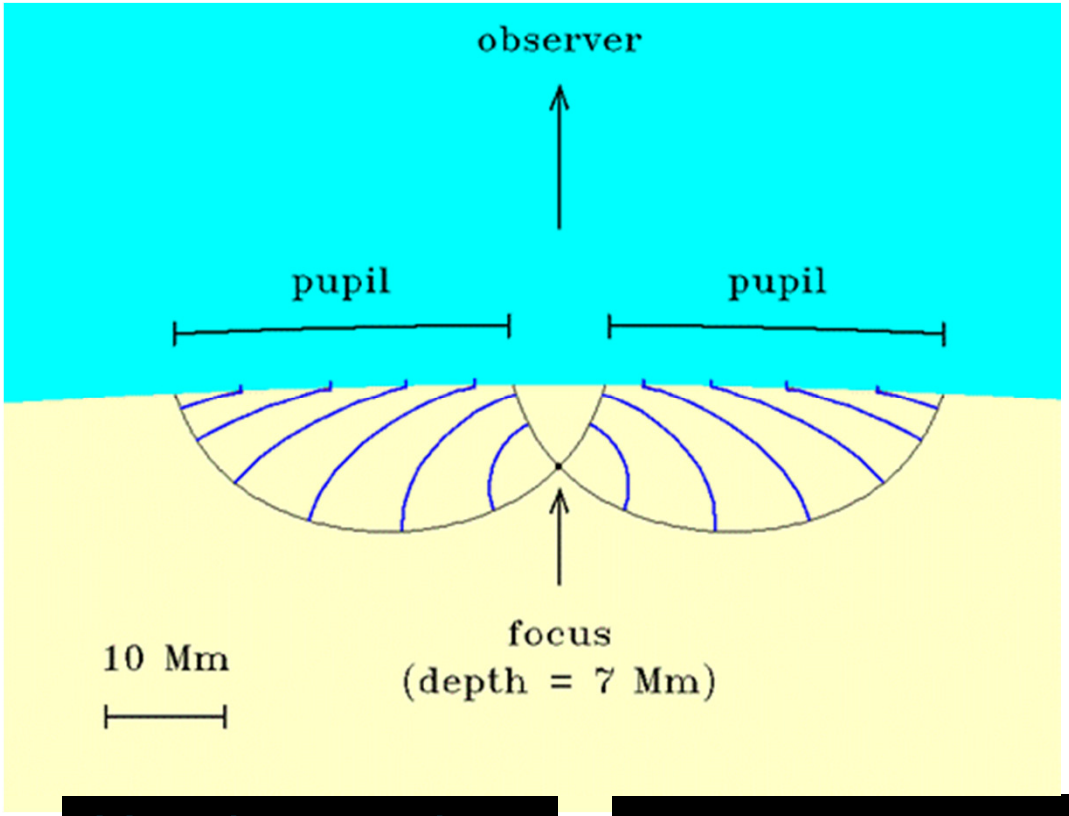

H_- = ingression

H_+ = egression

$$H_{\pm}(\mathbf{r}, z, t) = \int_P d^2\mathbf{r}' \; G_{\pm}(\mathbf{r}, \mathbf{r}', z, t)\, \psi(\mathbf{r}', t)$$

(z = depth, **r** = horizontal position of the focal point, ψ= surface amplitude, $G_{\pm}$= Greens' functions)

(Lindsey & Braun, 1990)

The ingression and egression power is sensitive to sources, sinks at focus.

Far-side imaging with helioseismic holography

Helioseismic holography is used to obtain images of solar active region on the far-side of the Sun by placing the focal point on the far-side surface.

The analysis on calculations of the phase shift (or equivalent travel time) between the ingression and egression signals.

1. egression, ingression:

$$H_{\pm}(\mathbf{r},z,\nu)=\int_P d^2\mathbf{r}'\; G_{\pm}(\mathbf{r},\mathbf{r}',z,\nu)\,\psi(\mathbf{r}',\nu)$$

2. correlation:

$$C(\mathbf{r},z,\nu)\equiv H_{+}(\mathbf{r},z,\nu)\;H_{-}^{*}(\mathbf{r},z,\nu)$$

3. correlation phase:

$$\varphi(\mathbf{r},z)=\arg\left(\left\langle C(\mathbf{r},z,\nu)\right\rangle_{\Delta\nu}\right)$$

4. travel-time perturbation:

$$\delta t(\mathbf{r},z)=\varphi(\mathbf{r},z)/2\pi\nu_{\circ}$$

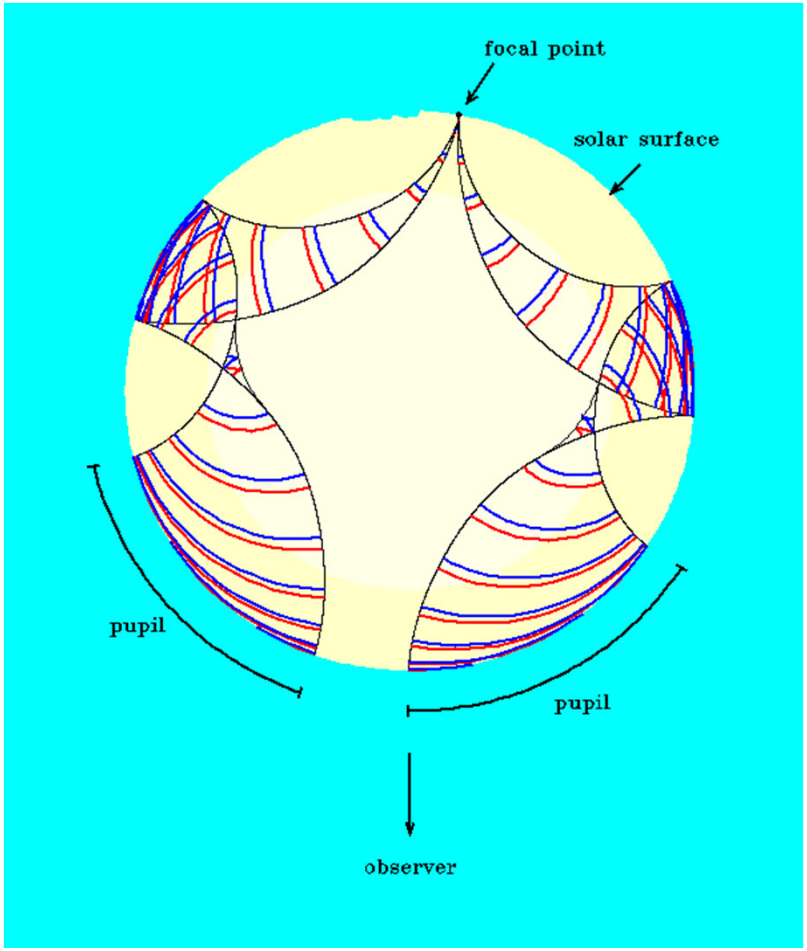

Lindsey & Braun 2000,
Science **287**, 1799

Daily far-side imaging data are used for space-weather forecasts because most solar storms are produced by active regions

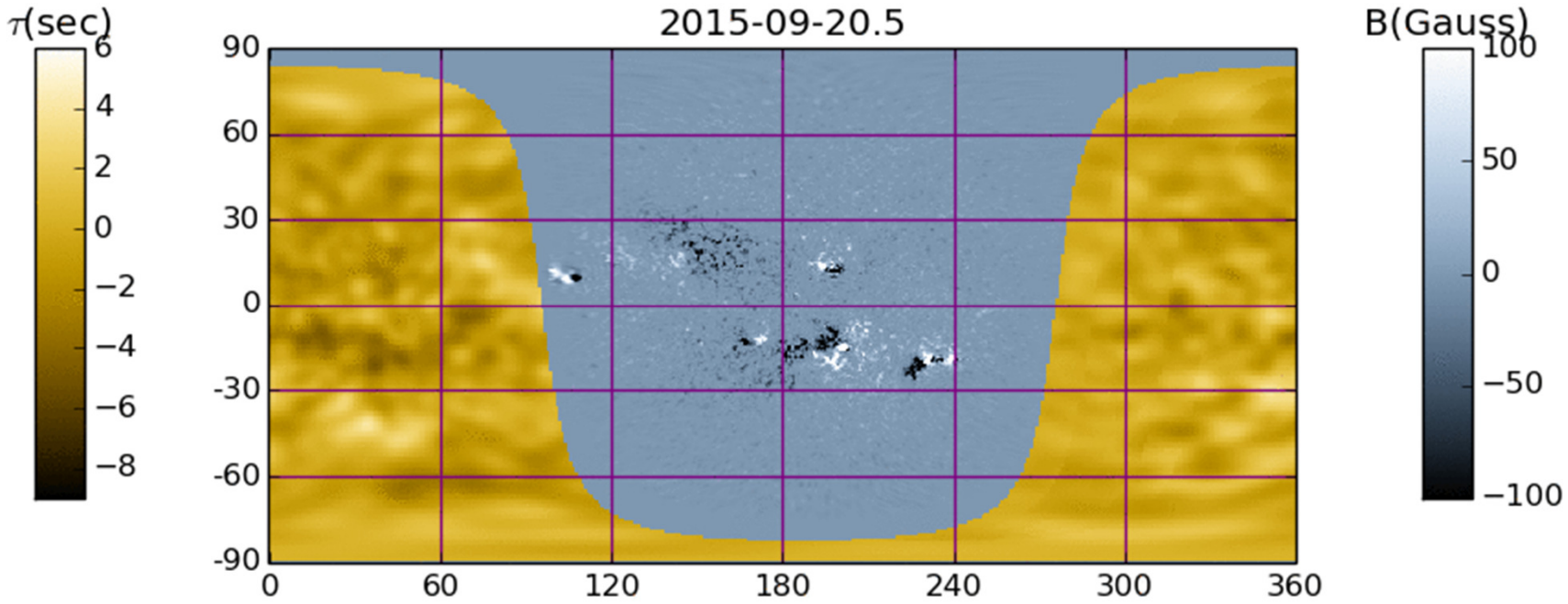

Composite Map of Far and Near Solar Hemispheres. Line-of-sight magnetic field in the Sun's near hemisphere is rendered in blue-gray, in Gauss. Seismic map of the Sun's far hemisphere is rendered in yellow. The far-side seismic image maps a phase shift between solar acoustic noise with periods of about five minutes embarking into the solar interior from the Sun's near hemisphere and its echos from respective locations in the far hemisphere. This phase shift is expressed here as a travel-time perturbation in seconds.

http://jsoc.stanford.edu/data/farside/

Results of time-distance helioseismology

Sunspot structure and dynamics

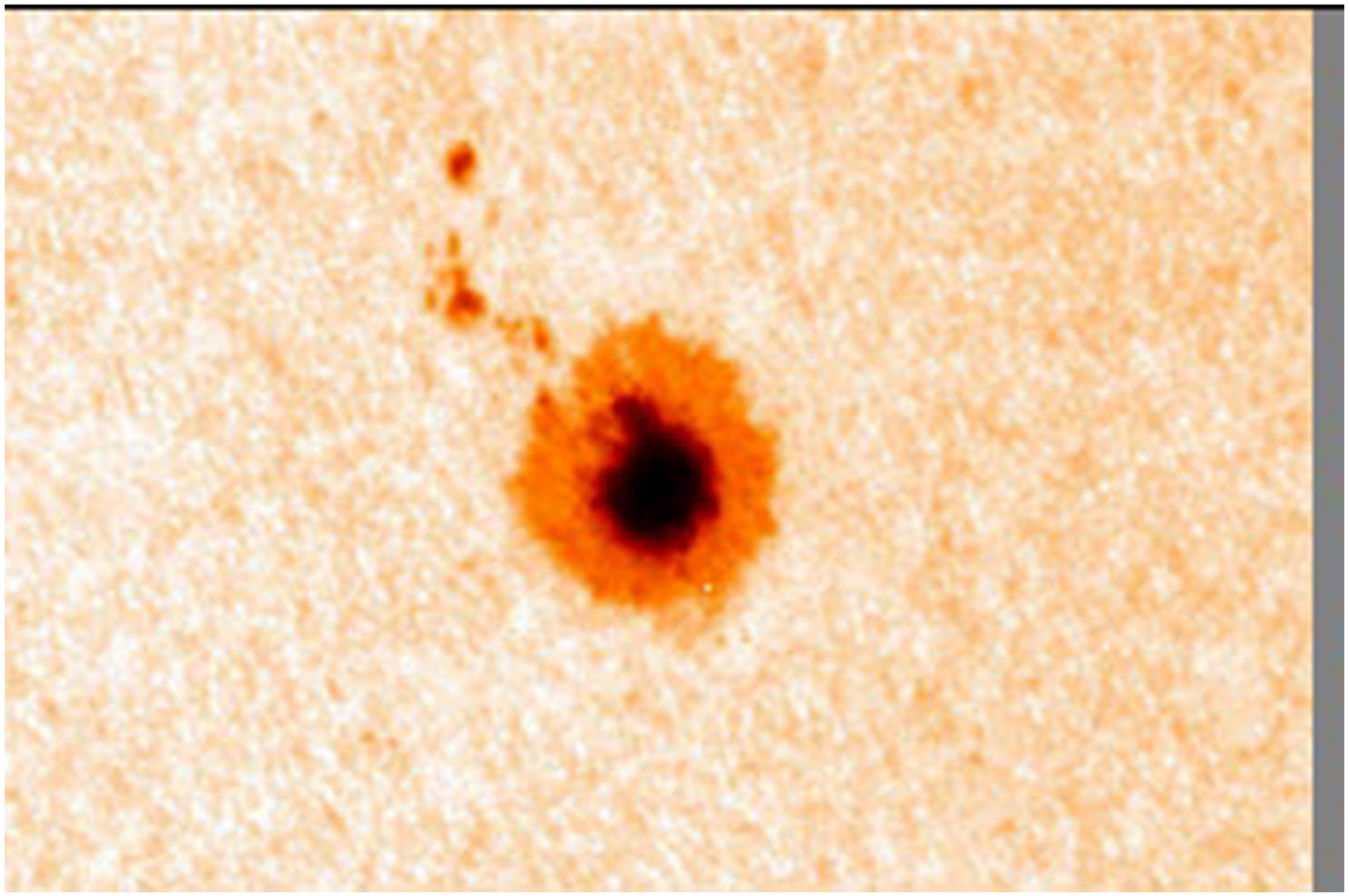

Numerical simulations of sunspot dynamics (N.Hurlburt)

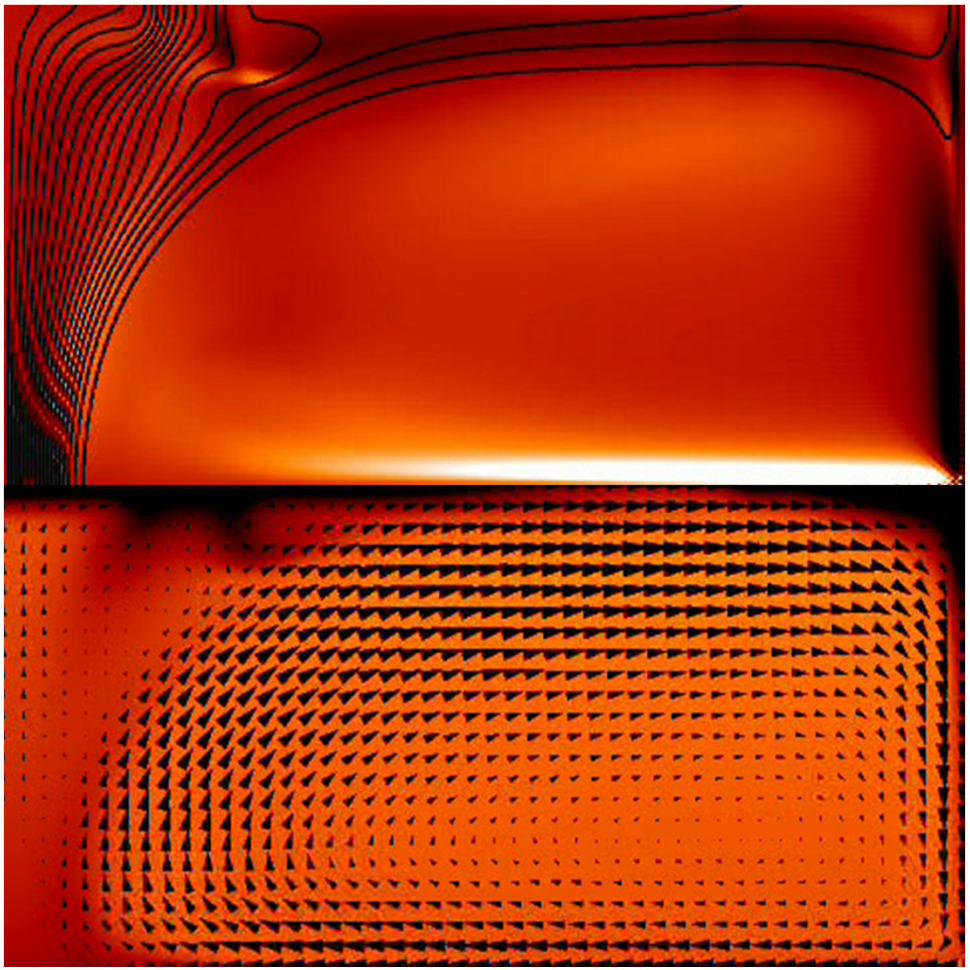

Numerical model of sunspot vs observations

Model **Observations**

Hurlburt and Rucklidge(2000)

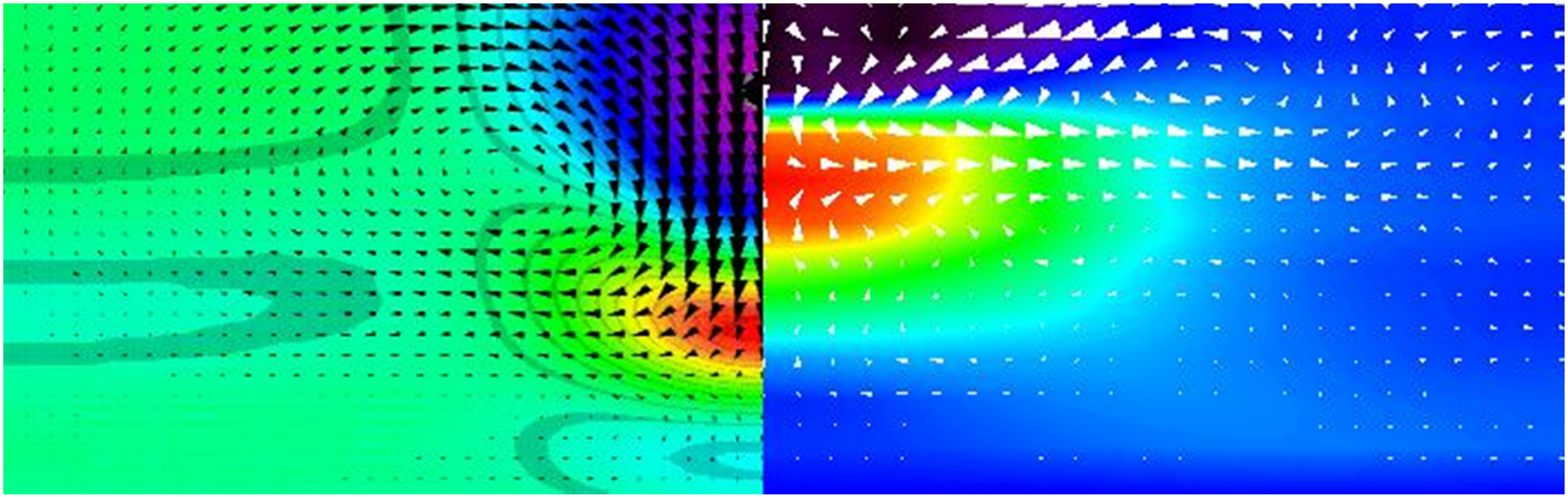

Flow patterns under the sunspot

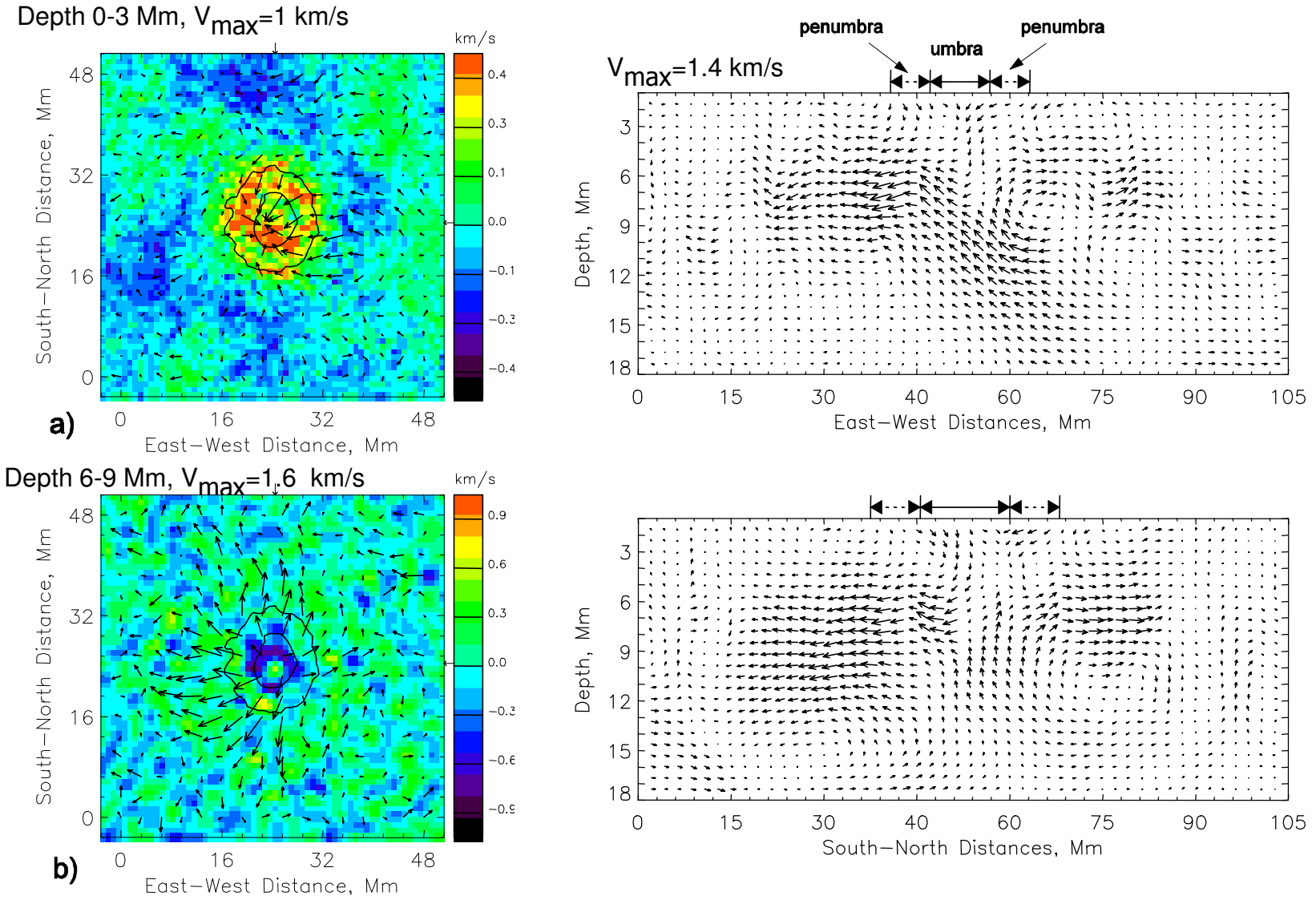

Parker's model of sunspots

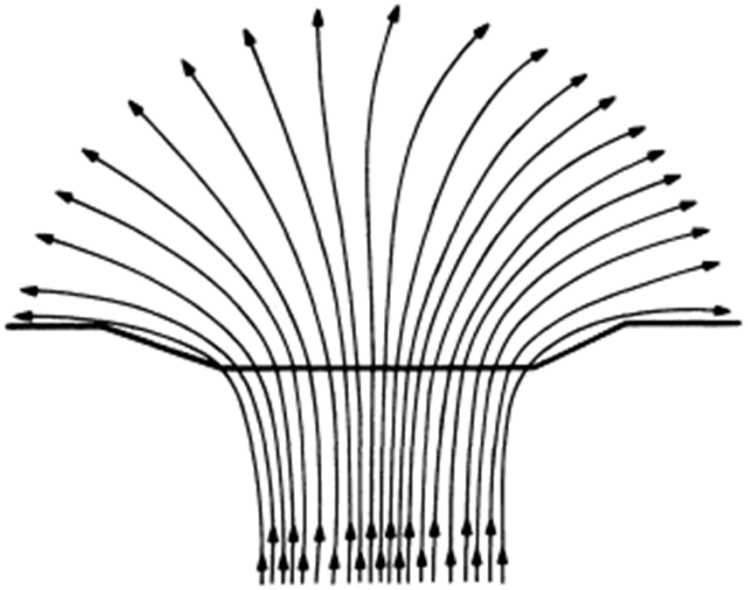

FIG. 1.—A sketch of the conventional idea of the magnetic field configuration of a sunspot. The heavy line represents the visible surface of the Sun.

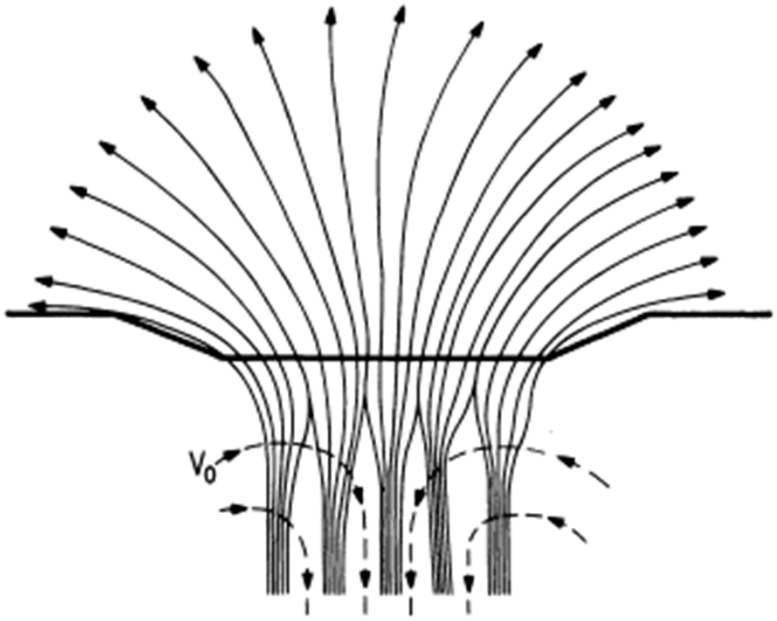

FIG. 2.—A sketch of the proposed magnetic field configuration, in which the field divides into individual flux tubes some distance below the visible surface. The dashed arrows represent the presumed convective downdraft which helps to hold the separate flux tubes together in the tight cluster that constitutes the sunspot.

Monolithic model

Cluster Model

Helioseismology provides strong evidence for the cluster model.

Subphotospheric imaging of active regions

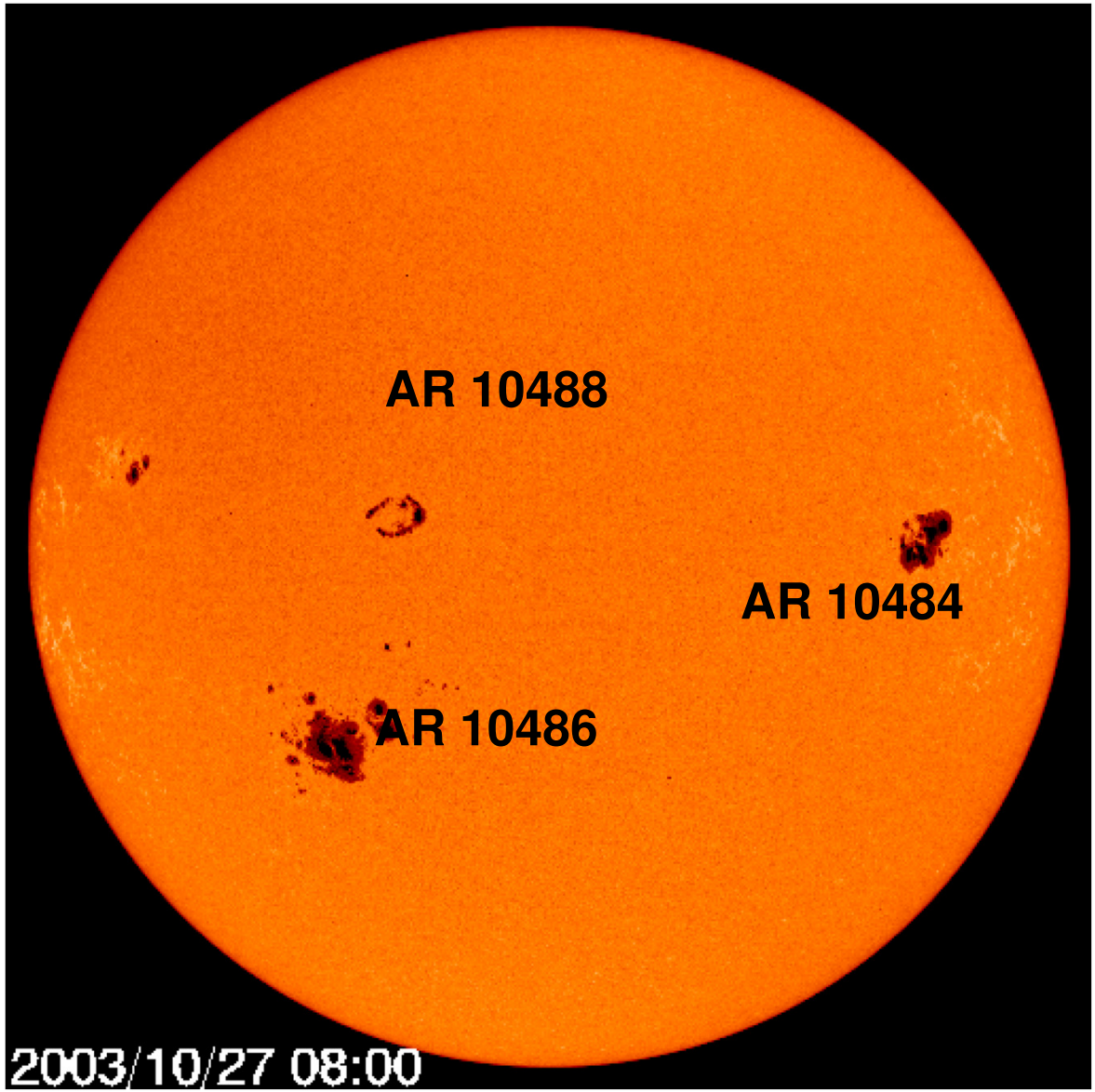

Evolution of AR 10486-488: October 24 – November 2, 2003

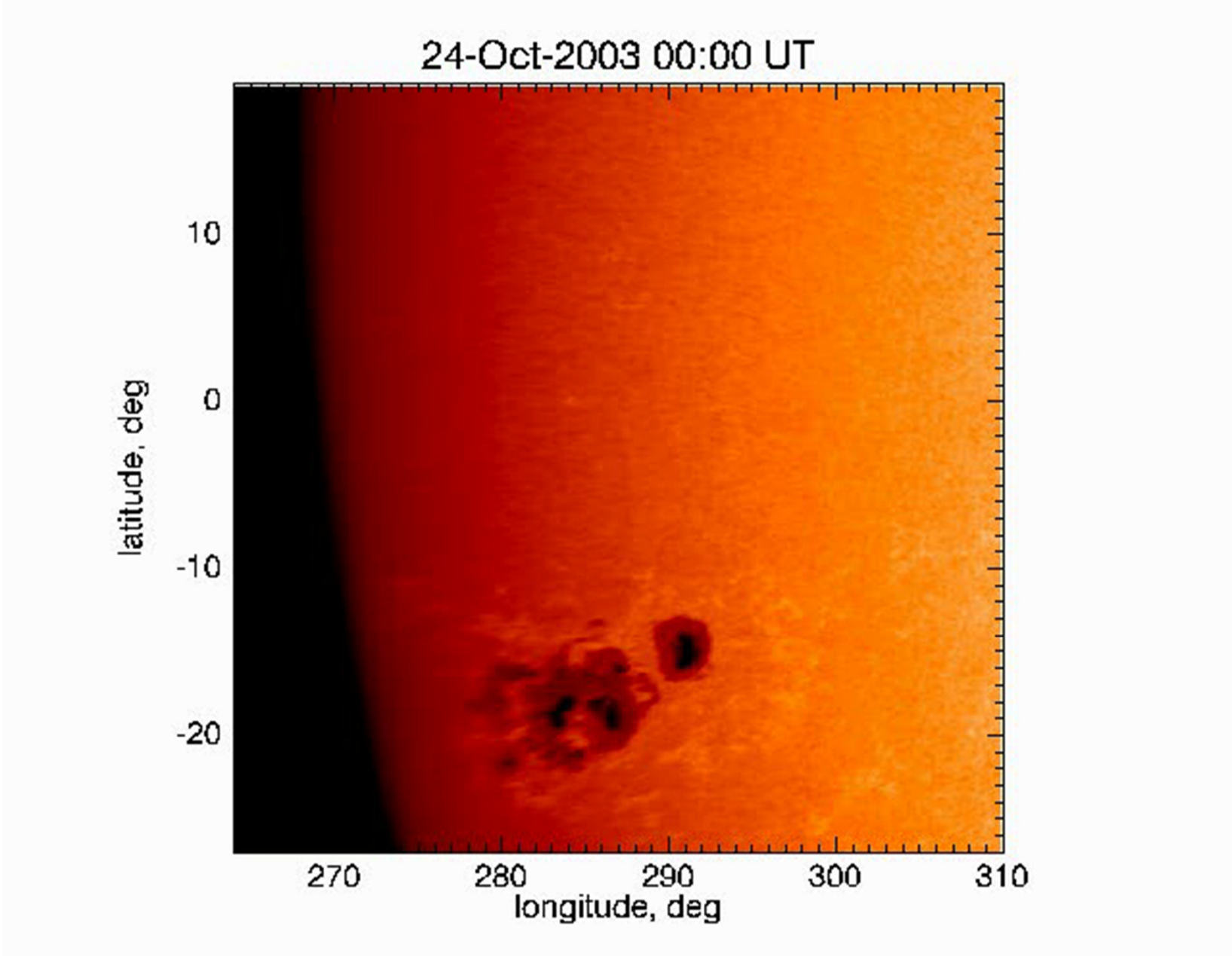

Sound-speed map and magnetogram of AR 10486 on October 25, 2003, 4:00 UT
(depth of the lower panel: 45 Mm)

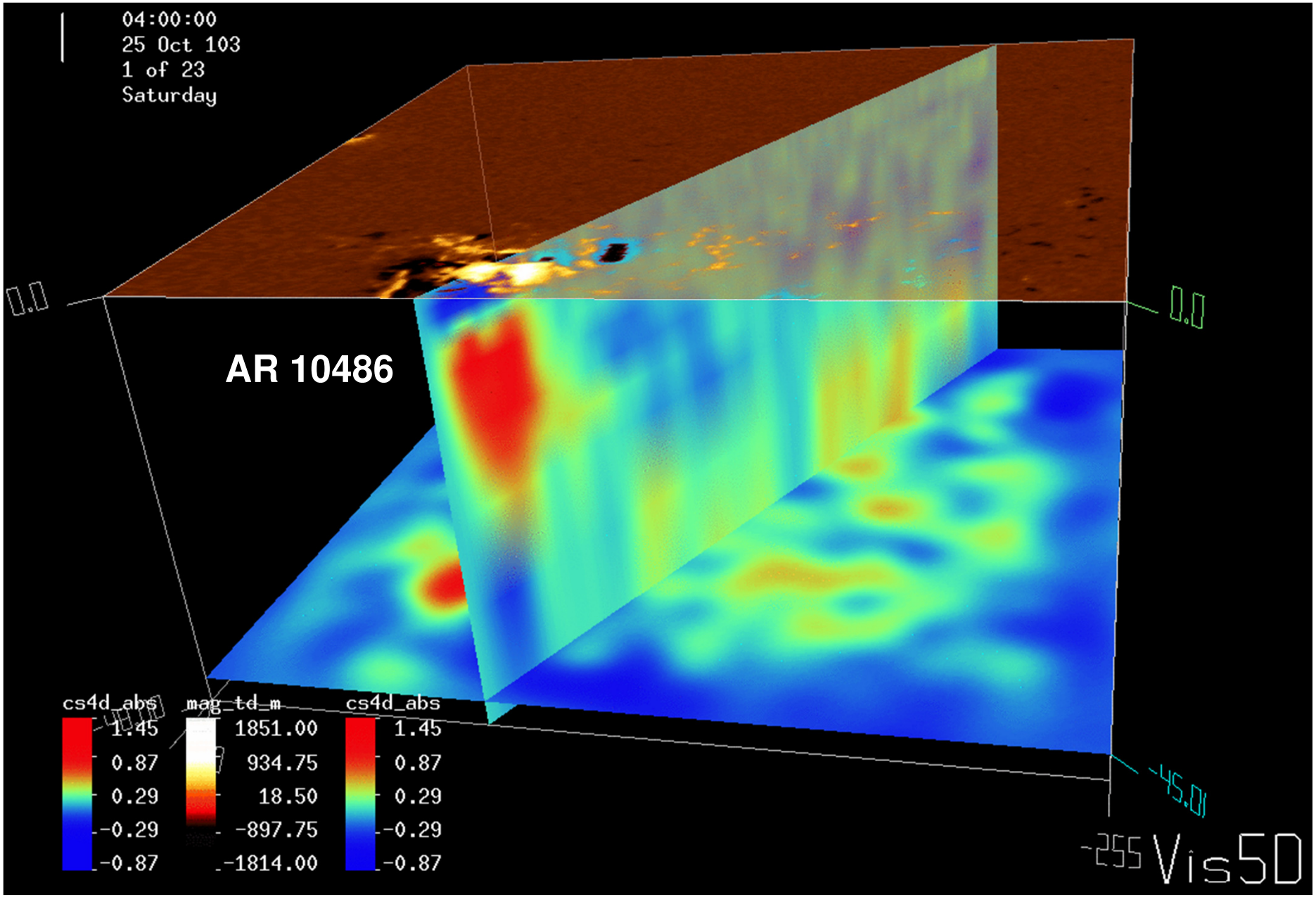

Sound-speed map and magnetogram of AR 10486 on October 26, 2003, 12:00 UT
AR 10488 is emerging

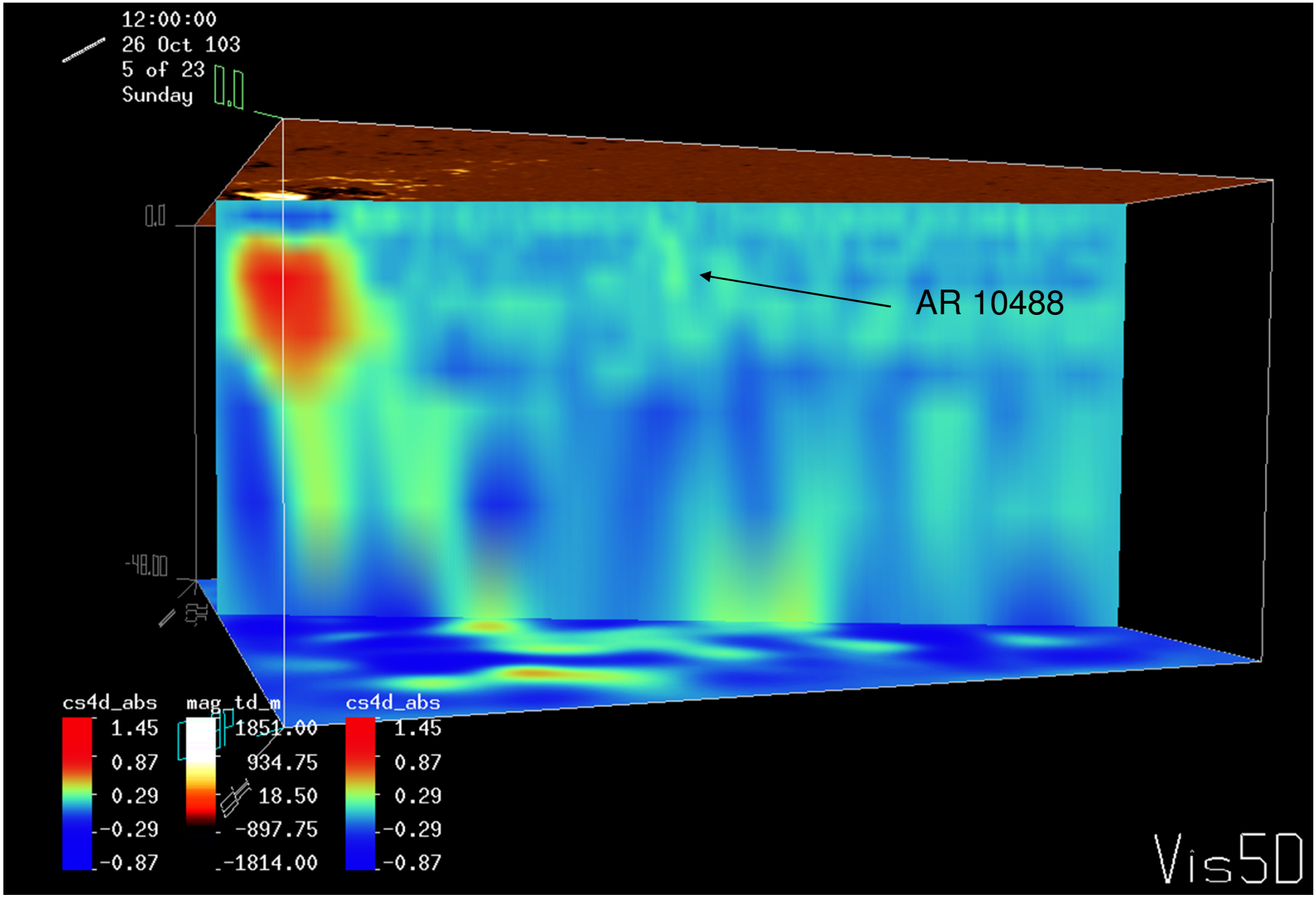

Emergence of AR 10488, October 26, 2003, 20:00 UT

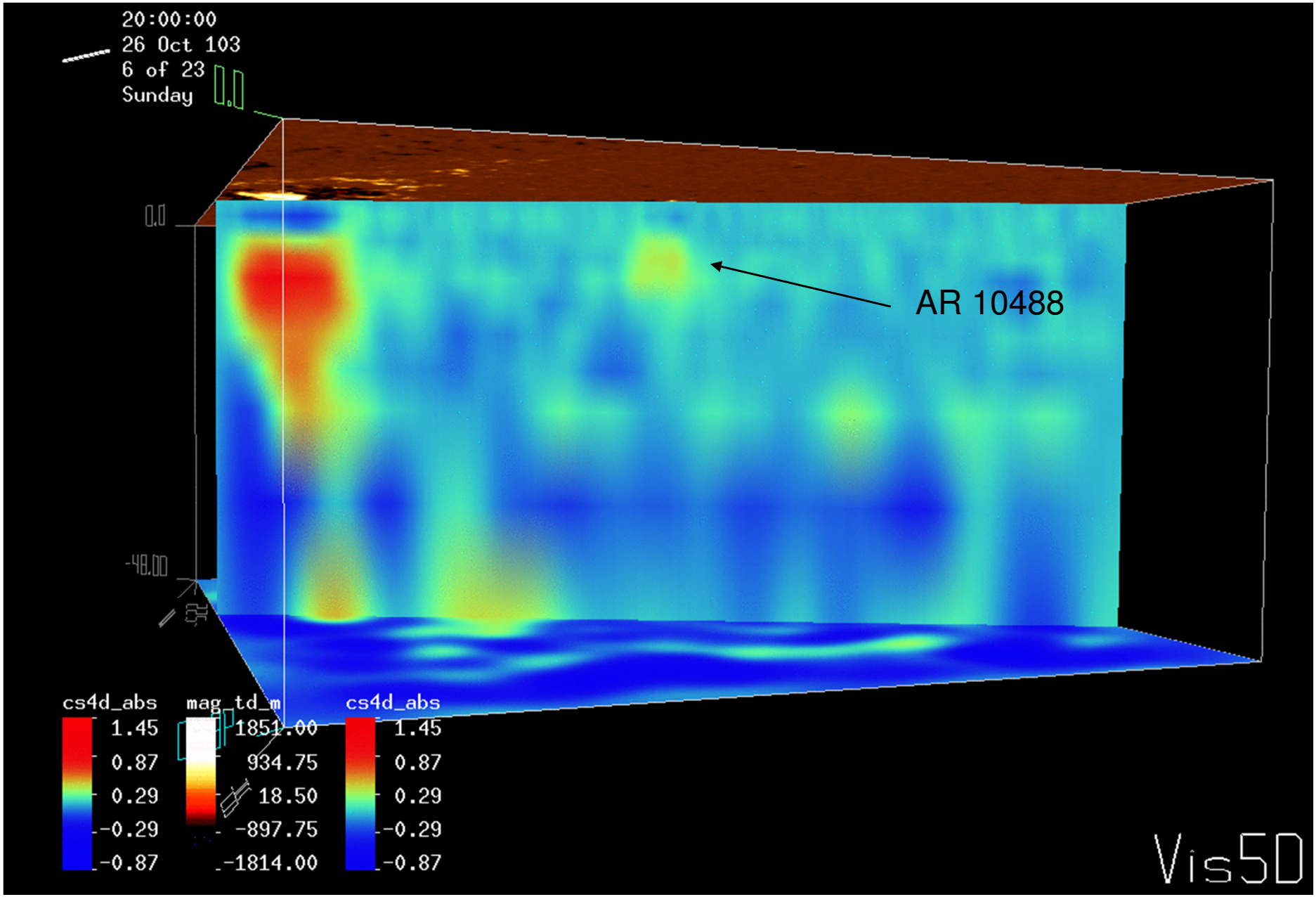

Emergence of AR 10488, October 26, 2003, 20:00 UT

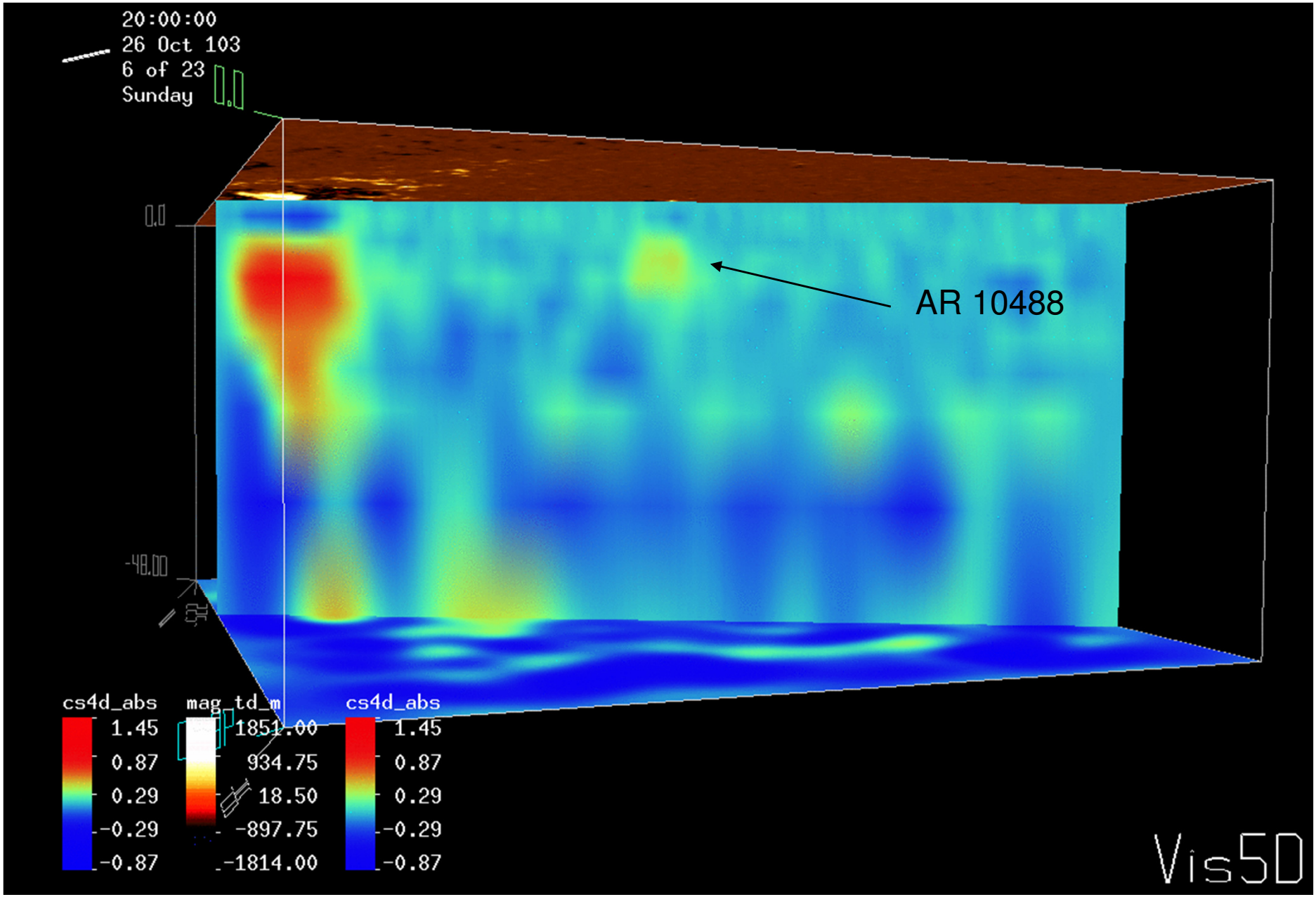

Emergence of AR 10488, October 27, 2003, 4:00 UT

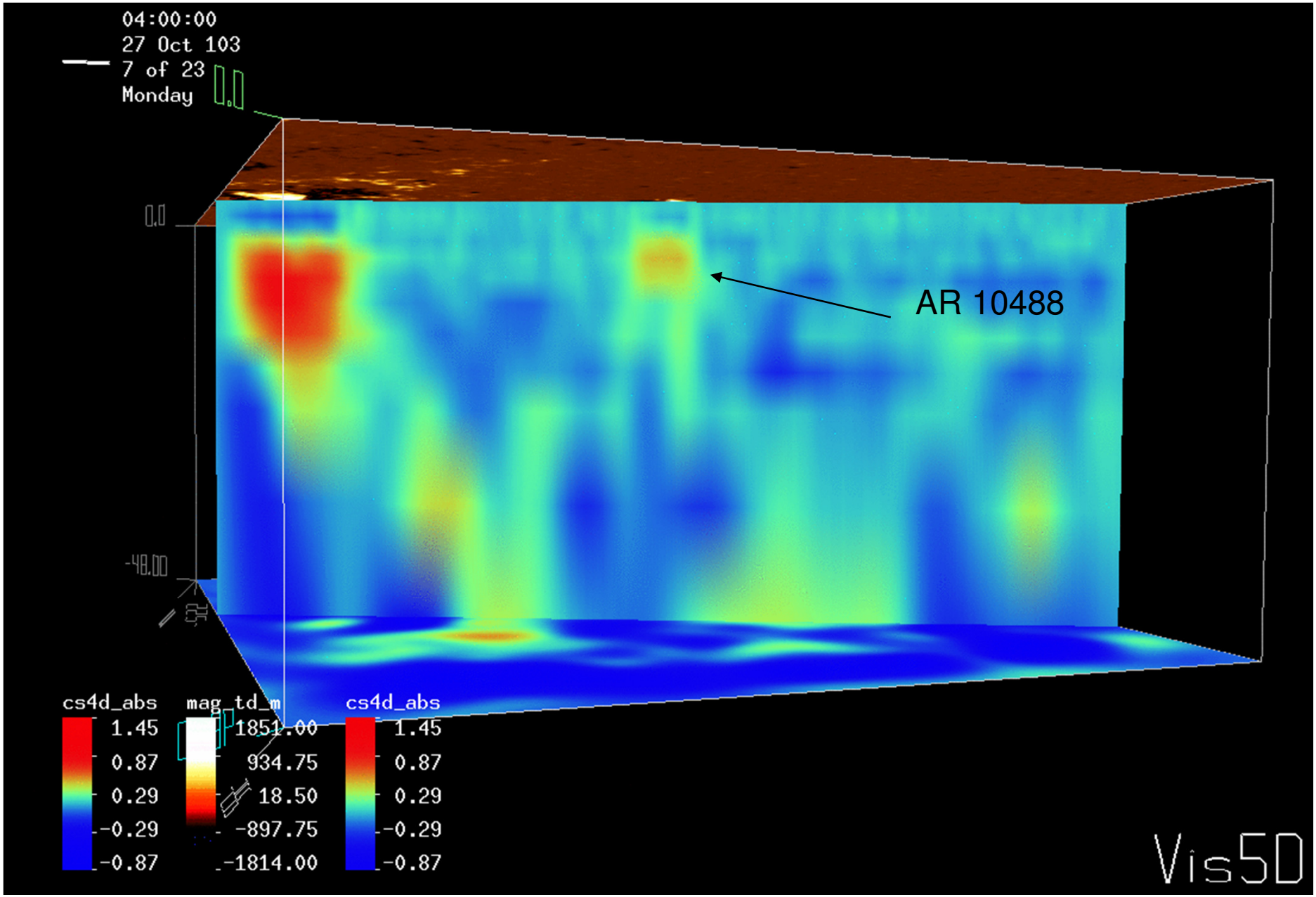

Growth and formation of sunspots of AR 10488, October 29, 2003, 4:00 UT

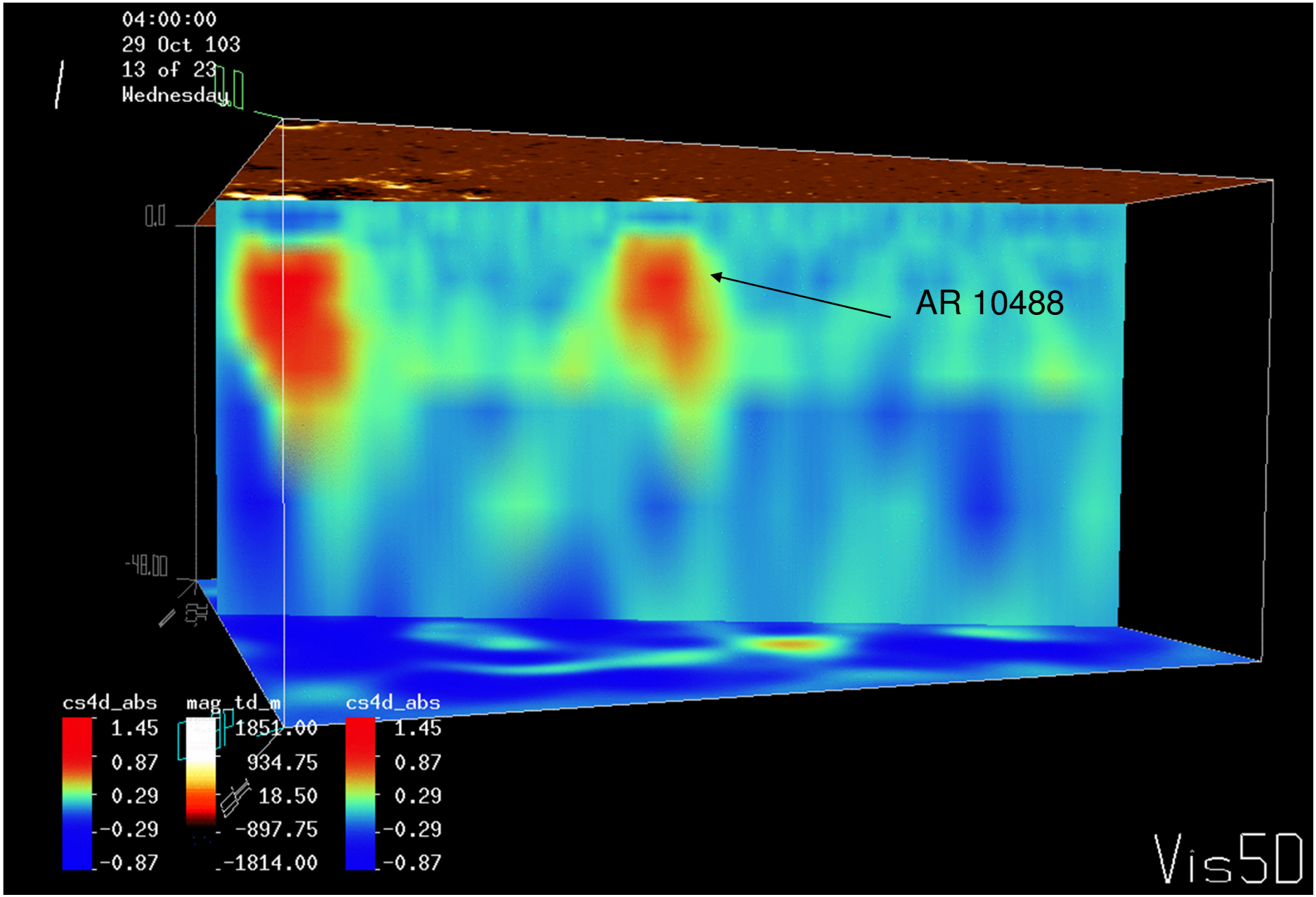

Growth and formation of sunspots of AR 10488, October 31, 2003, 12:00 UT

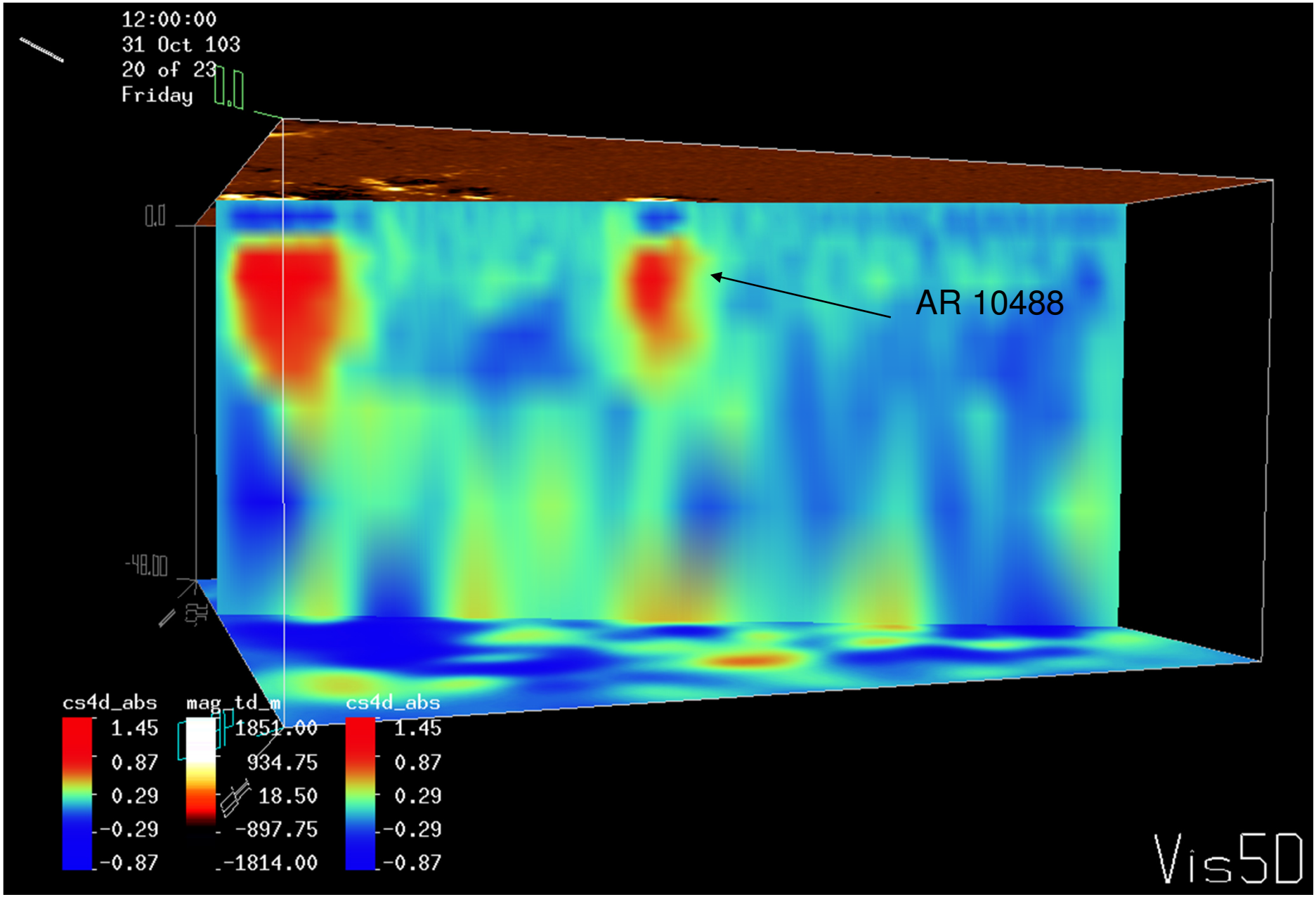

Cut in East-West direction through both magnetic polarities, showing a loop-like structure beneath AR 10488, October 30, 2003, 20:00 UT

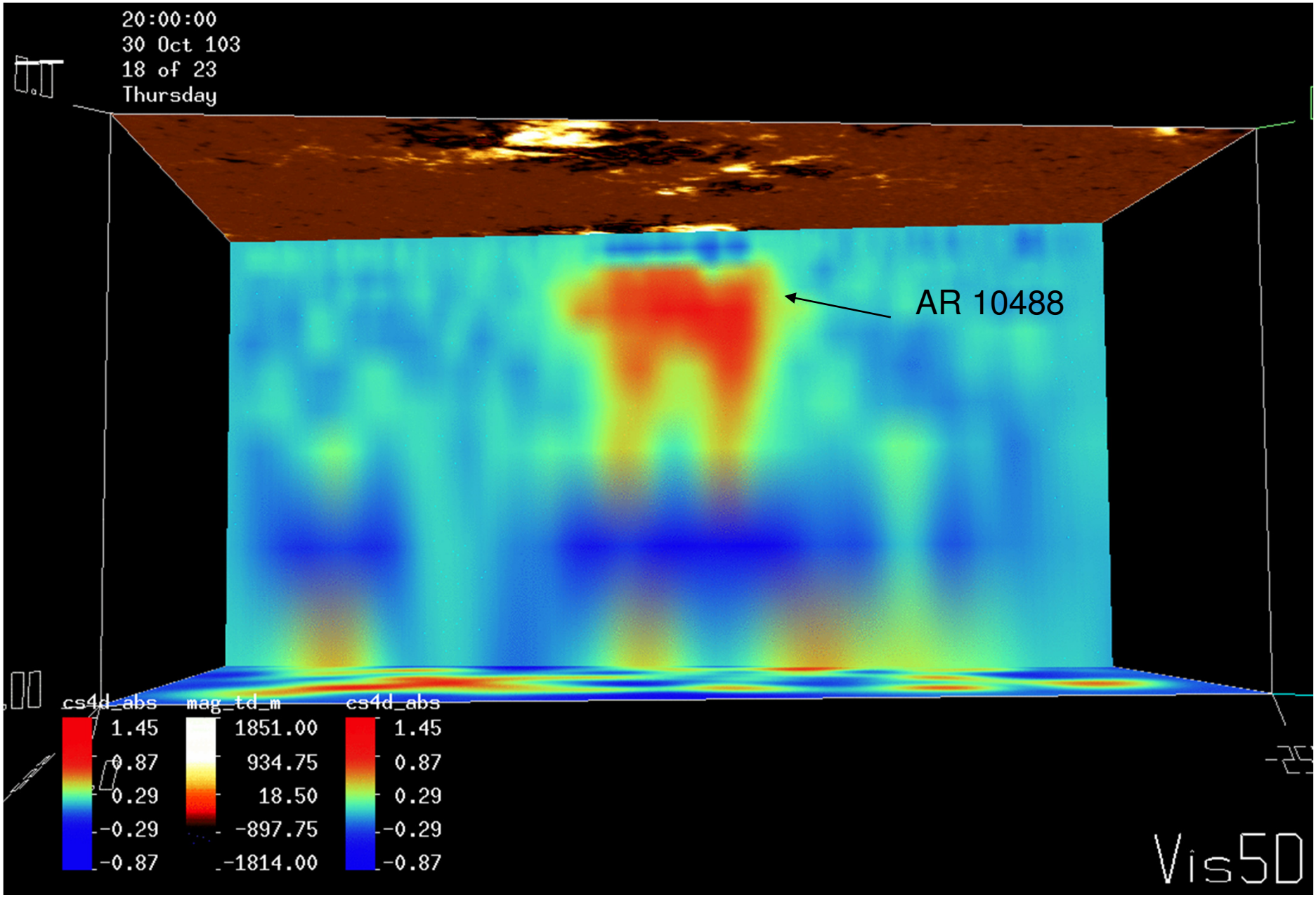

New helioseismology method of detection of emerging magnetic flux inside the Sun

Deep-focus Time-Distance Helioseismology: solar oscillation signal is filtered to select acoustic waves traveling to depth 40-70 Mm (right), averaged over arcs (left), and cross-correlated for opposite arcs. Travel-time perturbations are measured by fitting Gabor wavelet. This method has been tested with 3 different instruments (MDI, HMI, GONG) for many quiet and emerging flux regions.

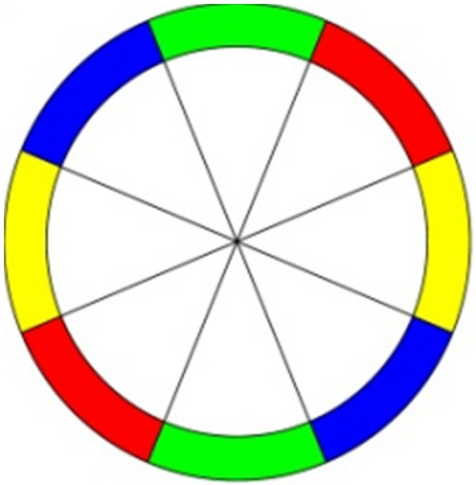

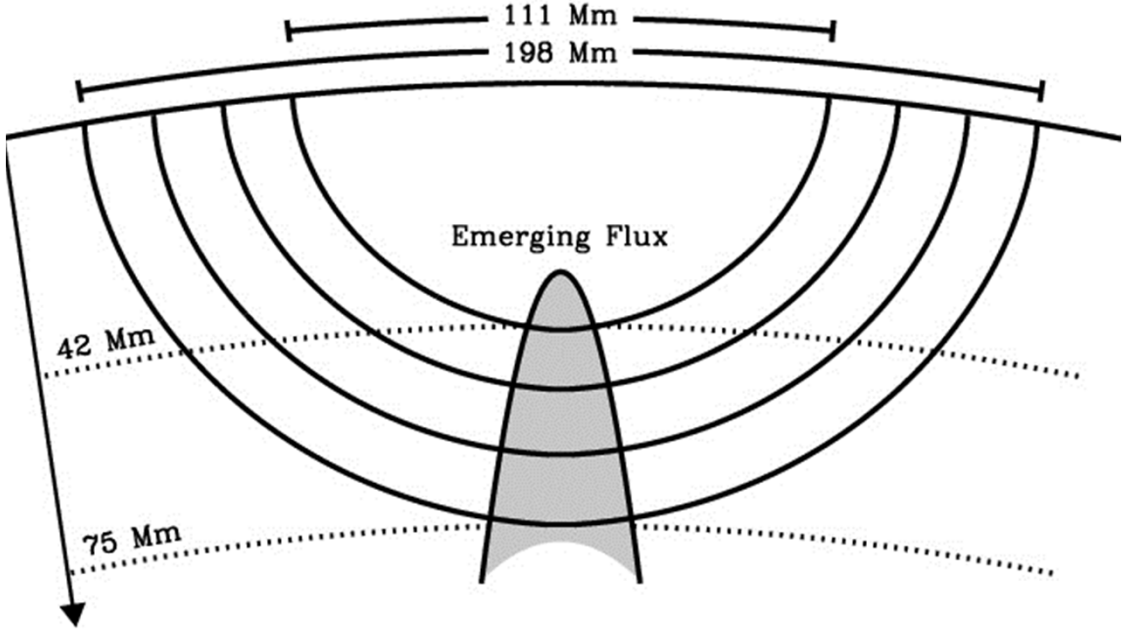

Ilonidis, Zhao, Kosovichev, 2011

Active region NOAA 1158, February 2011

- Detection of emerging active regions in the deep interior – 60-70 Mm below the visible surface, 24-hours before the flux appears on the surface.

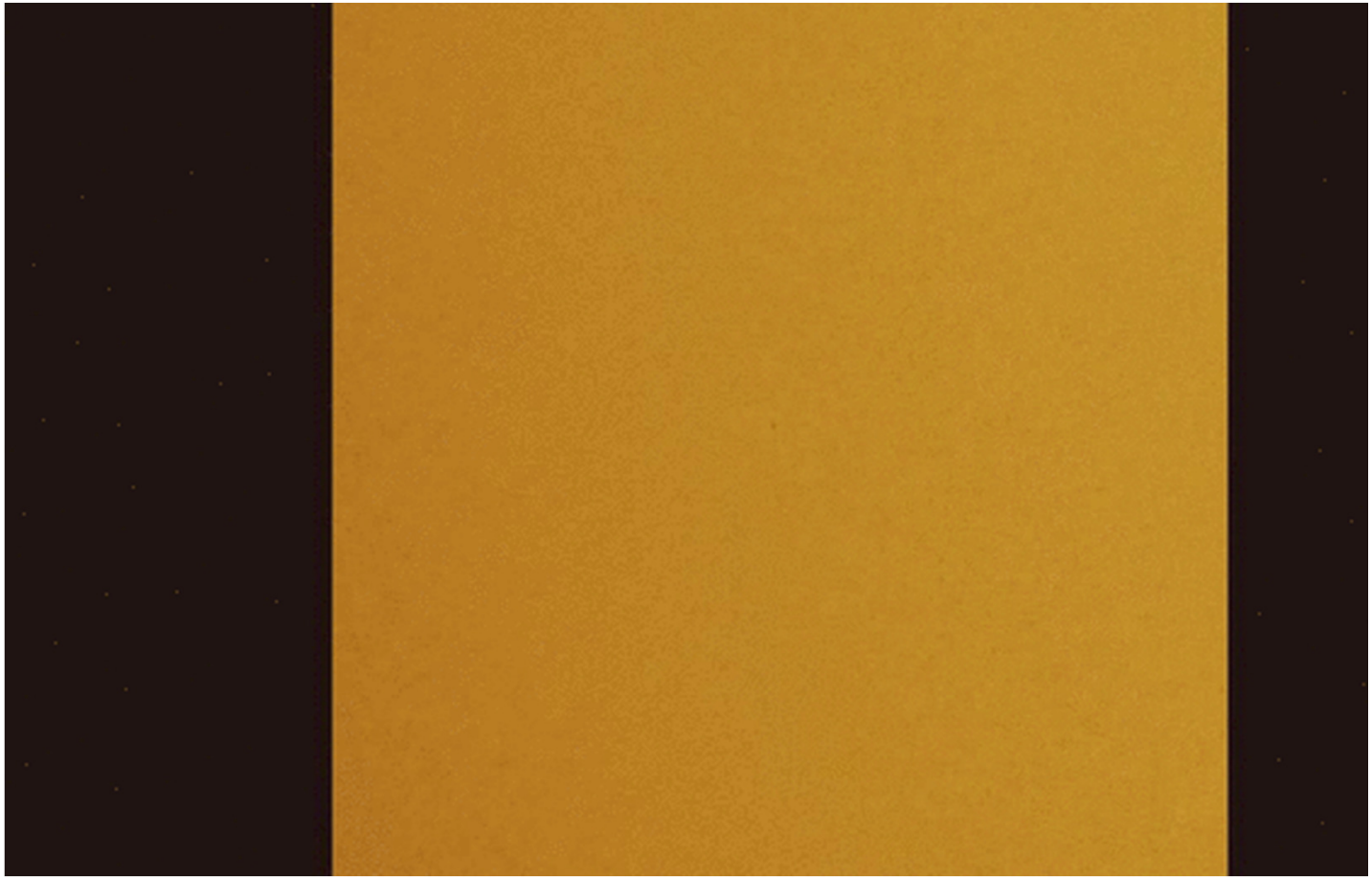

Synoptic subsurface flow maps from helioseismology analysis of Solar Dynamics Observatory data

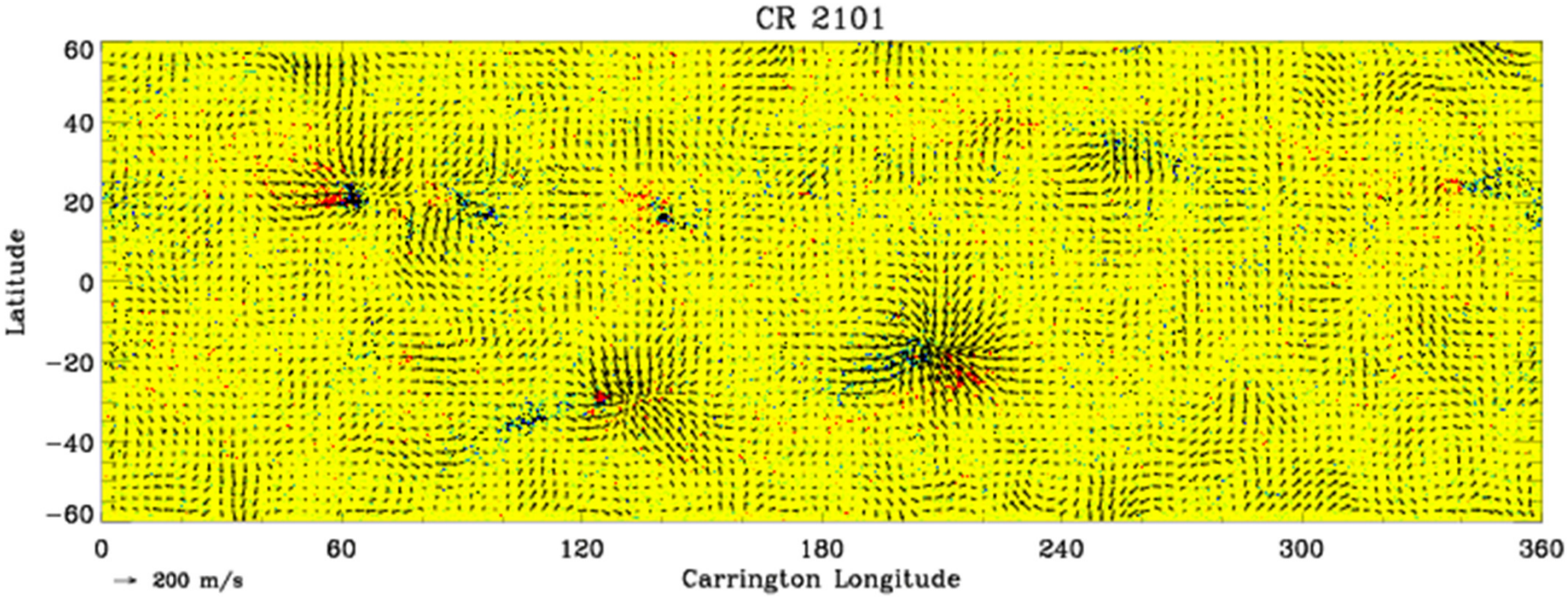

Large-scale converging flows with a speed of ~50 m/s affect the mean meridional flow (reduce its speed at high latitudes).

Measurements of deep meridional flows from SDO

- We used HMI full-disk Doppler observations, starting from May 1, 2010 through April 30, 2012, a total of 2 years' observations.
- Full-disk data are firstly binned down to 1024x1024 pixels. Running difference data are used for analysis.
- Deep-focusing time-distance helioseismology measurement is used.
- Fitting for acoustic travel times is done for each Carrington rotation. Then, fitted travel times are averaged over this 2-year period for the final results.

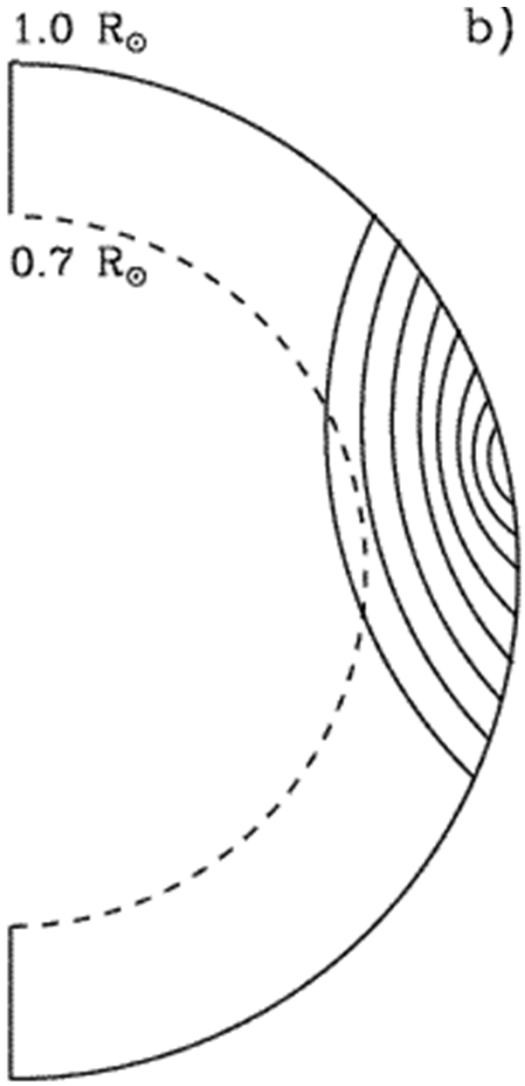

The helioseismology data do not support a single circulation cell needed for flux-transport dynamo

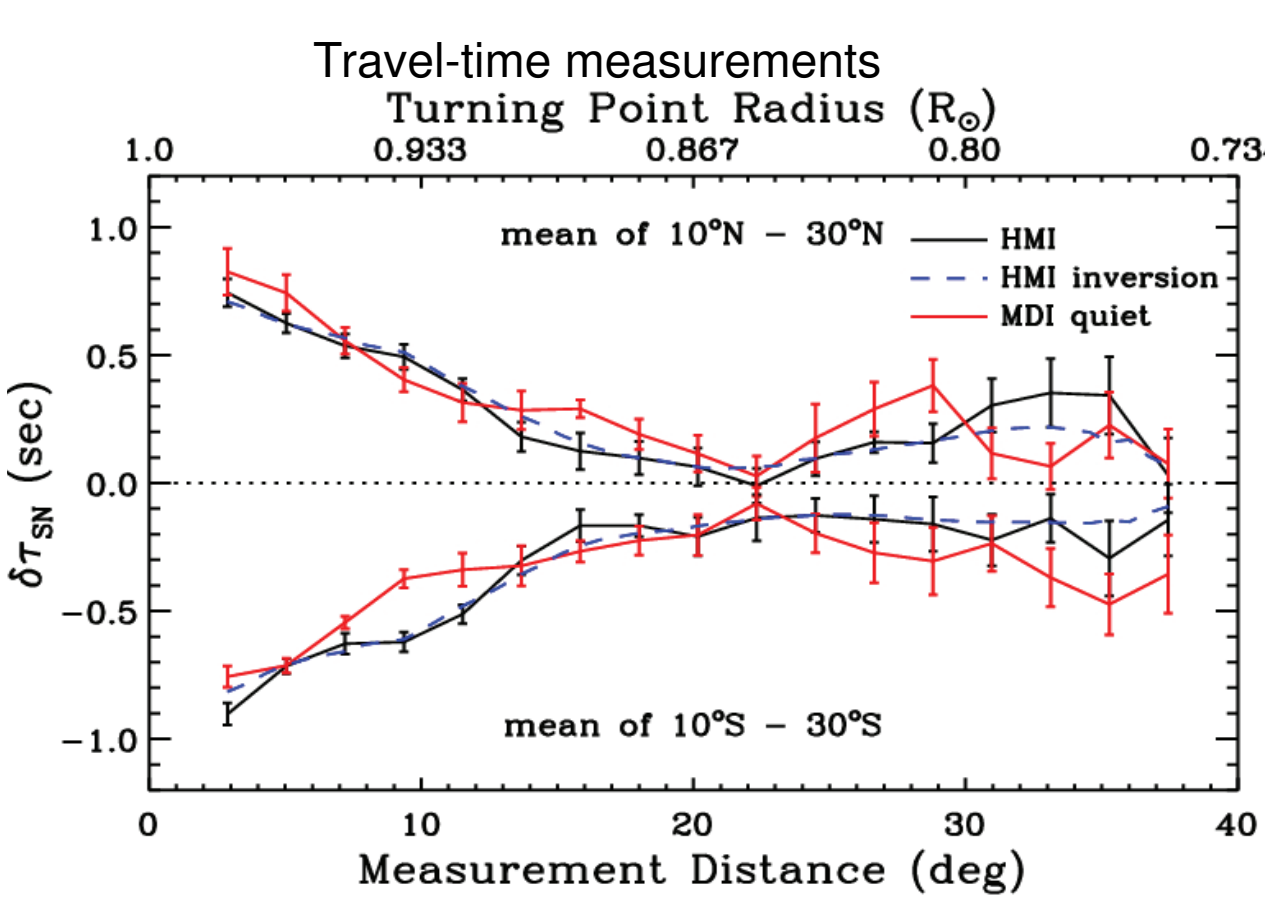

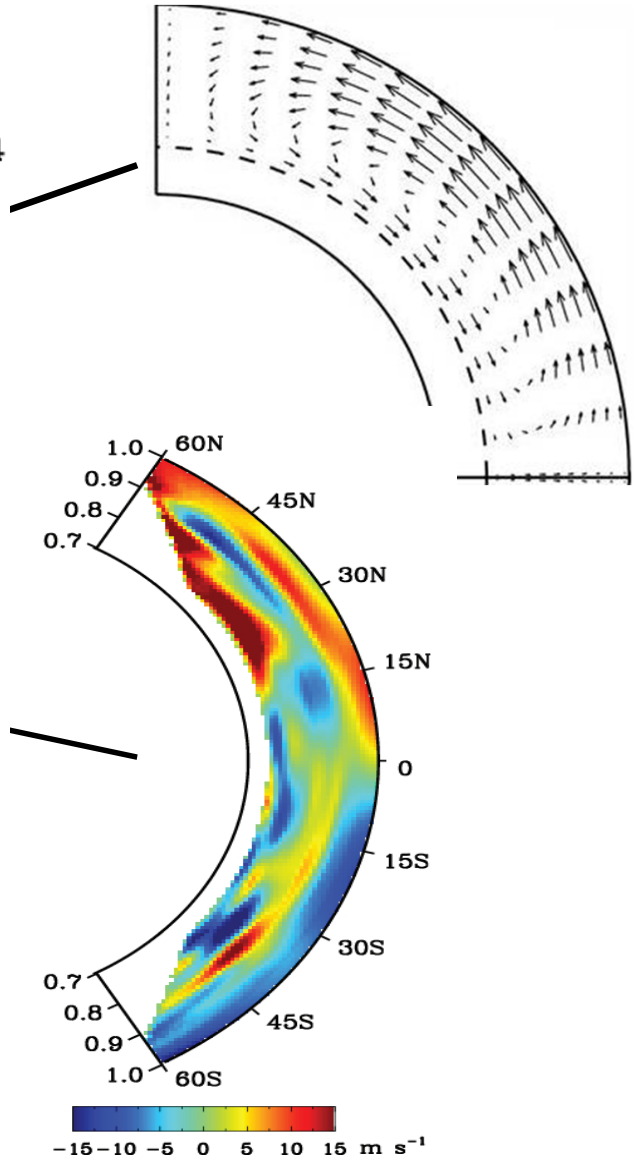

Inversion result

Zhao et al, 2013

Double-Cell Meridional Circulation from Helioseismology

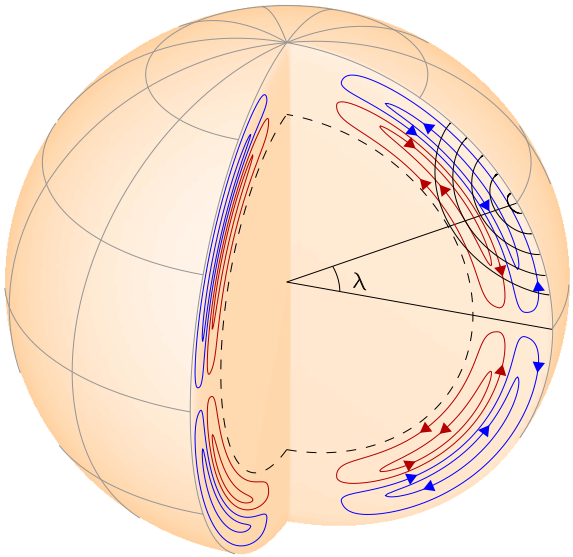

Zhao et al, 2013

The upper circulation cell extends from surface to about 0.83R (depending on latitude) , with the flow direction starting to change to equator-ward at about 0.93R (50Mm). Meridional flows switch to pole-ward again below 0.83R. The pole-ward flow near surface is an order of 15 m/s. The equator-ward flow below is an order of 10 m/s. The deeper pole-ward flow is roughly 10m/s.